# A COMPARISON OF FERROMAGNETIC PROPERTIES IN MICROWAVE, LOW FREQUENCY AND DIRECT CURRENT FIELDS

A.M. HALL, B.Sc., D.R.T.C.

THE ROYAL TECHNICAL COLLEGE, GLASGOW.



ProQuest LLC.
789 East Eisenhower Parkway
P.O. Box 1346
Ann Arbor, MI 48106 – 1346

CONTENTS:

LIST OF ILLUSTRATIONS.



21./

40./

ACKNOWLEDGEMENTS.

The work was carried out in the Electrical Engineering Department of the Royal Technical College. The author is indebted to Professor F.M. Bruce, who supervised the work; to Dr. H.R.L. Lamont for many valuable discussions during the later stages of the work; to Dr. E.S. Fairley for advice during the early stages; to the Department's Workshop for the manufacture of the resonator and other pieces of apparatus; and to the Telegraph Construction and Maintenance Co. Ltd. for the mumetal, radiometal and rhometal specimens.

SUMMARY

The thesis describes research work carried out at the Royal Technical College, on the measurement of microwave permeability, and of comparison measurements made with direct and $50^{c}/s$ fields.

Permeability may be defined both as a real and a complex quantity. The reasons for considering it complex are discussed and the relationships between the permeabilities obtained from measurements by different methods and the real and imaginary parts of the complex permeability is derived in a novel manner.

This is followed by a historical survey of published work which is considered important to the development of the technique used by the author.

In this the Q of a coaxial resonator with a 16 S.W.G. magnetic wire as inner conductor was compared with the Q of the same resonator with a copper inner conductor. From those measurements, the product of resistivity and permeability of the magnetic specimen was calculated. The design of the resonator was such as to allow a current to be passed through the specimen, lengthwise. This produced a magnetic/

magnetic field parallel to the microwave magnetic field, thus reducing the measured permeability. By using very strong fields, it was possible to estimate the value of the product of resistivity and permeability as the permeability tended to unity. This value is the resistivity and from it the permeability with no polarising field was calculated.

When the polarising field was varied in a cyclic manner, a hysteresis curve of permeability was drawn out. This curve has been called a "butterfly" curve by previous workers. The author's apparatus is somewhat simpler than that previously described and, as a new extension to this technique the author produced a similar type of curve using a field at right angles to the microwave field. This caused an increase in the resistivity-permeability product as the field increased, presumably due to an increase in resistivity caused by the perpendicular field. Curves were also produced with combined parallel and perpendicular fields.

For comparison purposes the resistivity and permeability were measured using d.c. The permeability was measured ballistically with a field applied lengthwise to the wire specimen by a long solenoid. It was realised that this/

this was not the same field configuration as that used in the microwave measurements, therefore a new technique was developed. In this, a $50^{c}/s$ alternating current was passed through the wire specimen and a reference specimen (eureka) in series. The voltage drop along each of these wires was compared by means of an a.c. potentiometer and the results of this comparison were used to calculate the complex permeability of the specimen. As the magnetic field was circular, it was of the same form as that used in the microwave measurements. The calculation of the permeability from these results required the extension of an existing proof of the voltage drop along a magnetic conductor to the case of one with a complex permeability. This extension introduced Bessel Functions of Complex Argument, which made the computation difficult. A family of curves was therefore drawn to ease this problem.

The rationalised M.K.S. system of units have been used throughout the thesis, except for some historical equations which have been quoted in their original units, and a suitable note added.

CHAPTER I.

FUNDAMENTAL APPROACH TO REAL & COMPLEX PERMEABILITY

(a) Static Fields.

The permeability of a substance may be defined by considering a large homogeneous specimen in a uniform magnetic field H. If B is the flux density produced in the specimen, then the relative permeability $\mu$ is given by

$$\mu \mu_0 = \frac{B}{H}$$

where $\mu_0 = 4\pi \times 10^{-7}$ H/m, is the permeability of free space. When the bulk product of a material is being considered it can be assumed that B is parallel to H and the permeability is therefore a space scalar.

It will be realised that an infinitely large specimen cannot be obtained in practice and that, in order to obtain reasonable accuracy with a specimen of convenient size, some form of compromise must be made. The specimen must be large enough to ensure that the flux density is uniform, assuming uniform field strength and a homogeneous specimen. However, if the specimen is short in the direction of the magnetising field, the poles induced at the end of it will reduce the flux density at the ends. This is known as self/

self-demagnetisation. For absolute accuracy the specimen should therefore be infinitely long. If the cross-sectional area of the specimen is reduced, however, the induced poles will be weakened. Thus, the accuracy is dependent on the ratio of length to cross-sectional area (or diameter). In ballistic measurements, with a relatively short search coil, Ewing[1] found that a wire specimen 300 diameters long could be considered as infinite.

Two other methods of overcoming this difficulty are as follows. In the first, a continuous magnetic circuit is formed by the specimen (e.g. a ring-shaped specimen forming the core of a toroid). This is very suitable for sheet material and it has also been used by Kreielsheimer[2] with wire specimens. This will be discussed more fully in Chapter VII. In the second method, a correction is made for self-demagnetisation, by calculating the field distortion which occurs. This can be applied to ellipsoidal shapes, but these are difficult to make as they require to be machined accurately. Although corrections can be applied for some other geometric shapes, they present the same difficulties as the ellipsoids.

Ferromagnetic materials, which were used in the experiments/

experiments to be described, exhibit the feature that their permeability is not constant for different values of applied field. It is therefore very difficult, in comparing various materials, to decide on a value of field strength at which comparative measurements should be made. In very low fields, however, the permeability varies almost linearly with the applied field strength, and in some materials it is constant. This feature enables the extrapolated value at H = 0 to be found. This provides a very convenient reference point and is called the "initial permeability" ($\mu'$)

Thus, $\mu' \mu_0 = B/H \quad \text{as } H \to 0$

The method of measurement will be described in Chapter VII.

Another marked feature of ferromagnetic materials is the hysteresis loop which is produced when the field strength is varied in a cyclic manner. The area of this loop is proportional to the work done in performing the cycle. This work done is known as the hysteresis loss and is important when considering a specimen subjected to alternating fields.

(b) <u>Alternating Fields - Low Frequency.</u>

At low frequencies the variation of permeability relative to the applied field strength is marked, and therefore all/

all measurements should include a reference to the field strength. A true statement of the magnetic properties must also include a reference to the hysteresis loss and, where applicable, to the eddy current loss caused by circulating currents within the material. This has been the usual method for many years, but there is a tendency now for these properties to be lumped together and specified by a complex permeability. This method has been fully discussed by McFadyen[3]. It is the concept used at high frequencies and is used throughout this thesis.

(c) Alternating Fields - Radio Frequency.

At high frequencies the concept of complex permeability has become well established since it was first proposed, in 1913, by Arkadiew[4]. The readier acceptance of this idea at radio frequencies than at power frequencies is probably due to the measurement techniques used at these frequencies. At radio frequencies, power loss measurement is difficult,and often impossible, and a measurement is therefore made of the attenuation and phase change produced when a wave is propagated into the material. This leads more easily to the concept of complex permeability. Theoretically it would be possible to convert this into a real/

real permeability and a power loss, but in practice, because of skin effect, it is difficult to define the volume in which this loss takes place. These factors necessitated the use of complex permeability which is, in fact, so convenient that it is now being used at low frequencies[3], where there are no such restrictions.

Before considering the theory of complex permeability, it is useful to derive the equations of electromagnetic propagation in a material of real relative permeability and to consider why these equations cannot be employed in the case of magnetic specimens. The following treatment, for real permeability, is that used by Sarbacher and Edson[6], but similar proofs are given in other standard textbooks.

First, consider the propagation of a plane wave into a material of conductivity $\sigma$ and having a real relative permeability, $\mu$. Let the propagation be in the Y direction and H in the Z plane, (fig.1) so that

$$H_z = H \quad \text{and} \quad H_x = H_y = 0.$$

Further, $\frac{\partial H_z}{\partial z} = \frac{\partial H_z}{\partial x} = 0$ since/

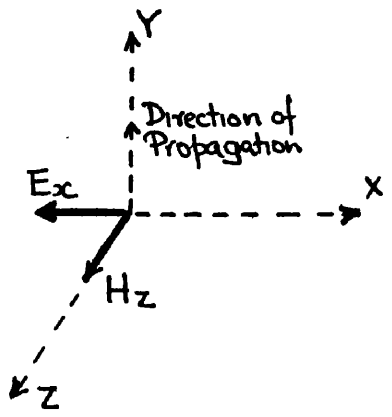

since the plane wave is in a medium of infinite extent.

Also, $$E_y = E_z = 0 \text{ and } E_x = -E$$

Then the wave equations

$$\left.\begin{aligned} \frac{\partial H_z}{\partial y} - \frac{\partial H_y}{\partial z} &= \sigma E_x + \epsilon \frac{\partial E_x}{\partial t} \\ \frac{\partial H_x}{\partial z} - \frac{\partial H_z}{\partial x} &= \sigma E_y + \epsilon \frac{\partial E_y}{\partial t} \\ \frac{\partial H_y}{\partial x} - \frac{\partial H_x}{\partial y} &= \sigma E_z + \epsilon \frac{\partial E_z}{\partial t} \end{aligned}\right\} \text{and} \left\{\begin{aligned} \frac{\partial E_z}{\partial y} - \frac{\partial E_y}{\partial z} &= -\mu_0 \mu \frac{\partial H_x}{\partial t} \\ \frac{\partial E_x}{\partial z} - \frac{\partial E_z}{\partial x} &= -\mu_0 \mu \frac{\partial H_y}{\partial t} \\ \frac{\partial E_y}{\partial x} - \frac{\partial E_x}{\partial y} &= -\mu_0 \mu \frac{\partial H_z}{\partial t} \end{aligned}\right.$$

reduce to $$\frac{\partial H}{\partial y} = -\sigma E - \epsilon \frac{\partial E}{\partial t} \quad \text{——— (1)}$$

and $$\frac{\partial (-E)}{\partial y} = -\mu_0 \mu \frac{\partial H}{\partial t} \quad \text{——— (2)}$$

Let $$H = H' e^{(j\omega t - \gamma y)} \quad \text{——— (3)}$$

and $$E = E' e^{(j\omega t - \gamma y)} \quad \text{——— (4)}$$

where $\gamma$ is the propagation constant of the wave in the Y direction.

Substituting (3) and (4) in (1) and (2), and dividing by $e^{(j\omega t - \gamma y)}$ it is found that

$$-\gamma H' = (\sigma + j\omega\epsilon) E'$$

$$\gamma E' = j\omega\mu_0\mu H'$$

Substituting this value of $H'$ in (5) and simplifying, gives

$$\gamma^2 = j\omega\mu_0\mu(\sigma + j\omega\epsilon) \quad \text{——— (6)}$$

Since $\sigma \gg \omega\epsilon$ then $\gamma = \sqrt{j\omega\sigma\mu_0\mu}$

$$\text{i.e. } \gamma = (1+j)\sqrt{\tfrac{1}{2}\omega\sigma\mu_0\mu} \quad - - - \quad (7)$$

since $(1+j)^2 = 2j$

From equation (7) it is seen that the propagation constant is complex; i.e. the wave experiences a reduction in amplitude and a displacement in phase. Denoting the attenuation constant by $\alpha$ and the phase constant by $\beta$ then, in conjunction with equation (7),

$$\gamma = \alpha + j\beta = (1+j)\sqrt{\tfrac{1}{2}\omega\sigma\mu_0\mu}$$

$$\text{i.e. } \alpha = \beta = \sqrt{\tfrac{1}{2}\omega\sigma\mu_0\mu} \quad - - - \quad (8)$$

The methods of measuring permeability will be discussed in Chapter II, but, basically, this equation applies to all the methods used at high frequencies. One would expect that, to find the permeability, either $\alpha$ or $\beta$ could be measured and then $\mu$ calculated from eqn.(8). Experimentally, however, it was found that the permeability calculated from $\alpha$ was not the same as that calculated from $\beta$ This led Arkadiew[4] to suggest that the permeability could be represented by a vector relationship of the form

$$\bar{\mu} = \mu_1 - j\mu_2 \quad - - - \quad (9)$$

which is a complex time vector, in the fourth quadrant, since it is found that the vector flux density usually lags the vector field strength by less than quarter of a cycle. In exceptional cases, such as ferromagnetic resonance, the permeability/

permeability lies in the third quadrant i.e. a phase lag of $90^{\circ}$ to $180^{\circ}$. Arkadiew followed this postulation by a proof of the relationship between the measured values and the real and imaginary parts of the complex permeability. A proof similar to Arkadiew's, but using modern notation, has been given by Millership and Webster[7], but it is felt that the following proof by the author, is more general.

Representing the values of permeability found by measuring $\alpha$ and $\beta$ by $\mu_R$ and $\mu_L$ respectively, eqn.(8) becomes;

$$\alpha = \sqrt{\tfrac{1}{2}\omega\sigma\mu_0\mu_R} \quad - - - - \quad (10)$$

$$\text{and } \beta = \sqrt{\tfrac{1}{2}\omega\sigma\mu_0\mu_L} \quad - - - - \quad (11)$$

Substituting the value of complex permeability from eqn.(9) for the real permeability in eqn.(6) and, assuming that $\sigma \gg \omega\epsilon$ then $\gamma^2 = j\omega\sigma\mu_0(\mu_1 - j\mu_2)$

Substituting for $\gamma$ and simplifying, the equation $(\alpha^2-\beta^2) + (2j\alpha\beta) = \omega\sigma\mu_0(\mu_2 + j\mu_1)$ is obtained.

Equating the real parts gives $\alpha^2-\beta^2 = \omega\sigma\mu_0\mu_2$ - - (12)

" " imaginary " " $2\alpha\beta = \omega\sigma\mu_0\mu_1$ - - - (13)

If the values of and given in eqns.(10) and (11) are now substituted in eqn.(13), the real part of the permeability is found to be

$$\mu_1 = \sqrt{\mu_R\mu_L} \quad - \quad \text{———————} \quad (14)$$

Similarly/

Similarly from eqn.(12),

$$\mu_L = \tfrac{1}{2}(\mu_R - \mu_L) \quad \text{---} \quad (15)$$

By manipulation of eqns.(14) and (15) it can be shown that

$$\mu_R = (\mu_1^2 + \mu_2^2)^{1/2} + \mu_2$$

and

$$\mu_L = (\mu_1^2 + \mu_2^2)^{1/2} - \mu_2$$

These four equations give the relationships between the measured values of permeability and the complex permeability.

## CHAPTER II.

### HISTORY OF HIGH FREQUENCY MEASUREMENTS.

Very complete bibliographies of measurements of permeability at frequencies over $100^{kc}/s$ are given by Allanson[8] in a paper on the permeability of ferromagnetic materials at frequencies in the range of $100^{kc}/s$ to $1,000^{Mc}/s$, and by Rado[9] in a paper which relates more especially to permeability at microwave frequencies. The following history discusses the main papers on which further work, by the present author, in the field of microwave permeability has been based. The chapter concludes with a table showing the frequency ranges covered by the papers discussed.

The earliest measurements on high frequency permeability were made by Arkadiew[5] in 1912. Using a spark gap oscillator he compared the reflection of an electromagnetic wave from a copper wire grating with that from a ferromagnetic wire grating, for frequencies in the range 100 to $20,000^{Mc}/s$. From the measurements of attenuation and phase displacement of the wave in each case, he calculated the values of $\mu_R$ and $\mu_L$ at these frequencies. Although radio measurement technique/

technique was still in its infancy, the quality of Arkadiew's research work is shown by the fact that his results are of the same order as more recent results. It is impossible to draw more accurate comparisons as the permeability of a specimen is very dependent on its exact chemical composition.

Although Kreielsheimer[2] made some important measurements at high frequencies ($300^{kc}/s$ to $6.5^{Mc}/s$ the next important experiments at very high frequencies were carried out by Hoag and Jones[10]. In these, the inductance of a lecher line was measured at frequencies between $470^{Mc}/s$ and $1350^{Mc}/s$. Since this involves, fundamentally, the phase constant, $\beta$ of the wave in the metal, the value of permeability calculated from it is $\mu_L$, The equation relating $\mu_L$ and the inductance, L, per unit length, was developed by Nicholson[11],

$$L = 4\log_e\frac{d}{r} + 4\frac{\mu_L}{x}\frac{\mathrm{ber}\,x.\,\mathrm{ber}'x + \mathrm{bei}\,x.\,\mathrm{bei}'x}{(\mathrm{ber}'x)^2+(\mathrm{bei}'x)^2} \qquad \text{(c.g.s. units)}$$

where L is the inductance in e.m.u./cm. of parallel wires d cm. apart, r cm. radius and resistivity $\rho$ ohm-cm.;

$x = 2r\sqrt{\frac{\pi\omega\mu_L}{\rho}}$;

and priming denotes the first derivative with respect to x.

A modification of the method used by Hoag and Jones was used by Glathart[12] at $197^{Mc}/s$. In place of a lecher line,

Glathart/

Glathart used a coaxial line with a magnetic inner conductor. By measuring the half wavelength, d, in the line and also the half wavelength, $d_o$, in free space, the inductive permeability can be calculated from

$$\mu_L = 1.256 \frac{a^2}{\rho} (\log_e \frac{b}{a})^2 \frac{(d_o - d)^2}{d_o d^4} \times 10^3 \qquad \text{(c.g.s. units)}$$

where a cm. and b cm. are the inner and outer conductor diameters and $\rho$ is the resistivity (ohm-cm) of the inner conductor. Two important advantages of the coaxial line over the lecher line are that errors due to stray fields are minimised and that, with a properly proportioned coaxial line, the difference between $d_o$ and d can be accentuated.

During the 1939-45 war, the advent of radar produced improved oscillators and measuring instruments for the centimetric and decimetric bands. Descriptions of several experimental methods using these new techniques have been published in the last few years. In Holland, Smidt[13], using Glathart's method, measured the permeability of drawn iron wire in the 360-580 Mc/s region. This was a measurement of $\mu_L$ only, but Smidt failed to point this out. He found that $\mu_L$ falls off very steeply with increasing frequency and states:

"One result which can be deduced from the very steep/

"steep falling off of the permeability is that the skin depth, which normally decreases with increasing frequency, increases again in the region of the fall. For the depth of penetration is given by

$$\delta = \sqrt{\frac{\rho}{2\pi\mu\omega}} \qquad \text{(c.g.s. units)}$$

and in the neighbourhood of the critical frequency, $\mu$ decreases more than w increases."

This argument is fallacious, since the measurements made were of $\mu_L$ and the skin depth equation relates to $\mu_R$.

Wieberdink[14,15] extended the method used by Smidt as follows. The specimen was again used as the inner conductor of a coaxial line which was fed from an oscillator by a loop coupling at one end. The other end was closed by a movable short circuiting piston. This piston had, at its face, a radially mounted loop with a detector connected to a galvanometer. The output of the detector with respect to piston position was of the form shown in fig.2. Wieberdink derived a relationship between the characteristic impedance of the line and the distances $(u_2 - u_1)$ and $(u_4 - u_3)$. By measuring these values and calculating the line impedance, the real and imaginary parts of the permeability of the inner conductor could also be calculated. The great advantage/

advantage of this method is that the measurement is independent of detector characteristic and does not require absolute measurements of detector current or frequency. The approximation is made that the losses in the copper outer conductor and those due to piston contact are negligible with respect of the losses in the wire specimen. This seems quite justifiable at the frequencies used, but at higher frequencies it might not be so,

The results of Wieberdink's[15] experiments show that, for a wire of composition 60% Ni, 40% Fe, a resonance occurs at approximately $320^{Mc}/s$ in which both $\mu_1$ and $\mu_2$ alter in a marked manner. Readings were taken over the range $266 - 375^{Mc}/s$ and the value of $\mu_2$ was found to rise to a peak, at $320^{Mc}/s$, which was approximately twice its value at $375^{Mc}/s$.

In all the above measurements, the conductivity of the specimen was assumed to be the same as the d.c. value. This was necessary, as it was impossible to separate permeability from conductivity in eqns.10 and 11. This assumption seemed to be supported by work carried out by Hagen and Rubens[16] in the infra-red region. Their experiments also showed that the permeability is unity in this region. Measurements/

Measurements made by Maxwell at a wavelength of 1 cm. (30,000 Mc/s) and Beck and Dawson[18] at a wavelength of 10 cms. (3,000 Mc/s) have shown, however, that the conductivity is affected by surface roughness, and it may not be possible to prepare the surface so that the h.f. conductivity has its d.c. value. Although Milner and Clayton[19] did not measure the absolute conductivity, they also showed that surface roughness played an important part in the apparent conductivity, at a wavelength of approximately 10 cms.

Johnson and Rado[20], in America, have overcome the problem of separating conductivity and permeability, in the following manner. A half wavelength, coaxial resonator, short circuited at both ends, was used with the specimen forming part of the inner conductor (fig. 3). At 200 Mc/s, for example, the specimen formed 17.75 cm. of the 74.5 cm. long inner conductor, the remainder being of brass. The diameter of the inner conductor was 0.159 cm. and of the outer, 1.59 cm. These dimensions were chosen mainly in order that

(a) most of the losses should take place in the inner conductor

and(b) the radius of the inner conductor should be large with respect to the skin depth in view of/

of certain approximations made in the derivation of permeability from a measurement of the Q of the cavity.

The value of the product of complex permeability and conductivity was calculated from a measurement of both the Q and the resonant frequency of the cavity. The authors found that altering the frequency of the oscillator exciting the cavity, in order to determine the resonance curve, caused errors due to frequency drift and change of the power output of the oscillator. The frequency was therefore maintained constant and the resonant frequency of the line altered by means of the movable dielectric bead shown in Fig. 3. From this a Q curve could be drawn.

In order to make the measurements independent of the conductivity of the magnetic specimen and of losses ih the rest of the resonator, the following ingenious method was used. The specimen was saturated by a circular static field produced by passing a high current (up to 1,000 A) through it. For this reason, the outer conductor had to be in two parts, separated by an insulated disc as shown. The product of conductivity and complex permeability is calculated from measurements of Q and resonant frequency with no externally/

externally applied field. If the specimen is now saturated, the permeability will be unity and the conductivity can be calculated. From this value and the results of the previous measurement, the complex permeability can be calculated. Unfortunately, owing to the heat produced, the saturation current cannot be maintained for long without affecting the conductivity and permeability of the specimen. An elaborate pulse method had therefore to be used. In this, a pulse of high current, sufficient to saturate the material, was passed through the specimen and the change of transmission efficiency of the cavity measured. This was measured relative to the Q and resonant frequency of the cavity with a low value of polarising current in the inner conductor, this Q having been measured by the point by point method already described. In some cases, such as soft iron, the current was insufficient to saturate the specimen and the saturation value had to be extrapolated from the highest current used.

Measurements were carried out on three specimens (pure iron and two types of Permalloy) at both 200 and 975 $^{Mc}/s$, the technique at the higher frequency being similar to that described, but with a 4 cm. long sample in a specially constructed resonator. Interesting experiments were also carried/

carried out on the effect of a varying polarising field. Cyclic variations of the field produced a curve (fig. 4), called a "butterfly" curve by the authors, which is really a form of hysteresis curve, as will be shown in Chapter V. The curve shown, relates the output voltage of the resonator to the value of the polarising current. The highest transmission or Q (i.e. the lowest permeability) occurs at the highest values of polarising current, which one would expect from a consideration of the incremental permeability of the low frequency hystersis loop. The dotted curve is obtained when starting from the demagnetised state, the full line curve representing the final, cyclic state. The slight assymetry was caused by heating.

This work by Johnson and Rado was a great advance on previous work, both in the care taken over the measurement procedure, and in the removal of errors due to the possibility of the conductivity not being the same as the d.c. value. It is unfortunate that no values of high frequency conductivity have been given in their published results.

In this country, over approximately the same period, work was being carried out at Leeds University on the measurement of $\mu_R$ over a wide range of frequencies (2,300 - 10,000 $^{Mc}/s$) by comparing/

TABLE I List of Permeability Measurements.

| REFCE. | NAME & DATE | RANGE OF MEASUREMENTS FREQUENCY Mc/S | RANGE OF MEASUREMENTS WAVELENGTH, CMS | METHOD | QUANTITY MEASURED |
|---|---|---|---|---|---|
| 5 | ARKADIEW 1919 | 100-20,000 | 300 - 1.5 | Reflection from wire grating | $\mu_R$ and $\mu_L$ |
| 10 | HOAG AND JONES 1932 | 135-470 | 220 - 64 | Inductance of lecher line | $\mu_L$ |
| 12 | GLATHART 1939 | 197 | 152 | Inducatance of lecher line (by line shortening i.e. $\lambda_o - \lambda$) | $\mu_L$ |
| 13 | SMIDT 1948 | 360-580 | 83 - 52 | " " | $\mu_L$ |
| 20 | JOHNSON AND RADO 1949 | 200 and 975 | 150 and 31 | Q and resonant frequency | $\mu_R$ and $\mu_L$ |
| 21 | HODSMAN et al 1949 | 2,300-10,000 | 13 - 3 | Attenuation | $\mu_R$ |
| 7 | MILLERSHIP AND WEBSTER 1950 | 150-1,500 | 200-20 | Attenuation of coaxial line and Glathart's method | $\mu_R$ and $\mu_L$ |
| 15 | WIEBERDINK 1950 | 260-375 | 115-80 | Standing Waves | $\mu_1$ and $\mu_2$ |

## CHAPTER III.

## PERMEABILITY IN THE 10 cm. REGION BY MEASUREMENT OF SKIN EFFECT.

### (a) Choice of Method.

Previous to the work to be described few measurements of permeability at microwavelengths had been made, as has been seen in the last chapter. The work of Milner and Clayton[19] on another problem, measurement of the effect of surface roughness at a wavelength of about 10 cm., gave the author the idea of extending the method to the measurement of permeability.

The method consists of the comparison of the Q of a coaxial resonator, having the specimen as inner conductor, with the Q of the same resonator with a reference specimen, copper, as inner conductor. Although Hodsman et al[21] have pointed out the difficulties of a Q measurement technique, it is felt that this method is adequate. An advantage of the coaxial resonator is that it has been possible to superimpose a d.c. magnetic field on the microwave magnetic field in an attempt to saturate the specimen, as described by Johnson and Rado[20], enabling the resistivity and permeability of the specimen to be separately calculated.

The/

The technique used by Milner and Clayton is as follows. The Q of a standard resonator, fig. 5(a), is compared with the Q of the test resonator, (b) containing the specimen. The standard resonator has an inner conductor slightly less than $\lambda/4$ long. This resonator is tuned to the resonant wavelength, $\lambda$ , by a dielectric introduced into the fringe field at the end of the inner conductor.

The test resonator has a $\lambda/4$ section similar to the standard, but with a hole drilled along its axis to allow the specimen to be introduced into the resonator. The specimen length is then adjusted until it forms the remaining $\lambda/2$ of the $3\lambda/4$ resonant system. This method of construction ensures that negligible loss occurs at the junction of the specimen and the resonator since there is no current flow at the $\lambda/4$ point.

In both the standard and test resonators, three coupling loops are introduced near the short circuited end. One of these is used to supply the power from the klystron through attenuating cables (fig. 6), to prevent interaction with the standard resonator. The second is connected to a crystal detector and the third is used to couple a length of lossy cable into either resonator. If the coupling of this cable/

cable is increased, the Q of the resonator is reduced.

The klystron is frequency modulated by $50^c/s$ ripple superimposed on the reflector voltage by connecting the heater winding in series with the reflector voltage (fig. 6). The detected output of each resonator therefore varies in amplitude with the change in frequency and, when this signal is applied to an oscilloscope with a suitable time base, a resonance curve is traced out. The two detected outputs are connected in antiphase (fig. 6) so that the oscilloscope displays the difference in the resonance curve. Using this difference curve, the resonant frequencies, "Q"s and amplitudes of the resonators are adjusted to be equal. The resonant frequencies are made equal by adjusting the dielectric in the standard resonator; the Qs are made equal by adjusting the loading on the standard resonator; and the amplitudes are adjusted by the coupling into the klystron resonator. When these are all equal, the difference curve will be a straight line.

When this balance point is reached, the resonance curve of the loaded resonator (the standard) is displayed on the oscilloscope and its height $h_t$ (corresponding to $Q_t$) is noted. The loading cable is now removed and the height $h_o$ (corresponding to $Q_o$) of th resonance curve without loading, is/

is noted. Allowing for the square law of the detector,

$$\frac{Q_o}{Q_t} = \sqrt{\frac{h_o}{h_t}}$$

(This and the following relationship, which were stated, without proof and not in exactly the same form, by Milner and Clayton will be discussed and proved in Chapter IV)

If the test specimen (resistivity $\rho_t$ , permeability $\mu_t$ , radius $a_t$ ) is replaced by a reference specimen ($\rho_r$ , $\mu_r$ and $a_r$) a similar expression for the new Q of the test resonator, $Q_r$, can be obtained. The ratio of $Q_r/Q_t$ and hence $\frac{\rho_t \mu_t}{\rho_r \mu_r}$ can then be calculated from

$$\frac{a_r}{a_t}\sqrt{\frac{\rho_t \mu_t}{\rho_r \mu_r}} = \frac{Q_r}{Q_t}\left(\frac{k a_r}{\sqrt{\rho_r \mu_r}} + 1\right) - \frac{k a_r}{\sqrt{\rho_r \mu_r}} \quad \text{---} \quad (16)$$

In the following experiments copper was used as a reference specimen.

(b) <u>Initial Experiments on Skin Effect Measurements</u>.

Resonators similar to those used by Milner and Clayton were built, and measurements attempted using magnetic conductors. At first, the only oscillator available for the supply of 10 cm. power to the resonators was a CV35, high voltage klystron, but this proved unsuitable due to its poor frequency modulation characteristic. It was found that a sweep/

sweep of about $50^{Mc}/s$ was required to trace the resonance curves and this could not be obtained by varying the reflector potential of the CV35. A low voltage klystron (707B) similar to that used by Milner and Clayton was obtained and this was found to have a suitable modulation characteristic.

When measurements were made using a lossy specimen (i.e. low Q of test resonator) it was found impossible to balance the difference of the resonator outputs, as viewed on the oscilloscope, to a straight line. A considerable residue remained in many cases due to differences in the shapes of the standard and test-resonator curves. At first this was thought to be due to differences in the characteristics of the detectors, either the loops and associated capacities or of the crystals themselves. Experiments were made in changing crystals and redesigning the holders. The three types of mounts are shown in fig. 7.

Types (a) and (b) are probably similar to those used by Milner and Clayton. Two of type (c), a photograph of which is seen in fig. 11, were made to give positive or negative outputs depending on whether a British (CV101) or American (IN2I) crystal was used. The difference in these crystals/

crystals is in the direction of current flow through the crystal, i.e. in the convention of whether the "base" of the crystal is connected to the large or small diameter end. The dimensions of these crystals are almost identical. Experiments were carried out with the four crystal mounts using different crystals, but, although improvements could be obtained it was found impossible to remove the unbalance. The main difficulty in these attempts lay in the fact that the results could not be judged quantitatively, only qualitatively. The most suitable components were used and other sources of distortion studied.

It was felt that the irregular nature of the ripple modulation on the reflector did not produce a true picture of the resonance curve, thus masking the nature of the difference curve. A transitron-miller time base was therefore built up to improve the linearity of the frequency sweep. This circuit is shown in fig. 8, where V2 is the transitron-miller valve which produces a linear time sweep at a repetition frequency of 50 $^{c}/s$. This rate is decided by the 2M ohm variable resistor in the grid circuit and the sweep is synchronised to the mains supply by the amplifier V1 whose grid is connected to the heater voltage. The oscilloscope

can/

can also be synchronised to the mains frequency, giving a steadier trace. This more linear sweep helped in the interpretation of the curves and improved the accuracy of balance.

Another slight improvement was obtained by situating the detector coupling loop $\lambda/2$ from the short-circuited end, while the input coupling was situated, as usual, near the short-circuited end. This reduced the direct coupling between the loops, improving the shape of the Q curve. The combined effect of these improvements was not sufficient to allow the method to be considered accurate and it was therefore decided to redesign the resonators.

Apart from the difficulty of balancing out, a disadvantage of the test resonator is that the specimen is fixed at one end and free at the other. It is thus impossible to ensure that the specimen is rigid and straight. If the specimen bends, distortion of the field occurs, which may give rise to errors in the calculation of resistivity from the Q of the resonator. Thus it is desirable to have the specimen fixed at both ends, therefore a resonator was designed one wavelength long, with the specimen held at each end by a quarter wavelength line. This resonator will be described/

described fully in part (c) of this chapter.

While studying the effect of the bent inner conductor, several interesting features were noted which support the desirability of the new resonator. As they are not essential to the measurement technique they will be described in Appendix II.

(c) Modified Technique for Microwave-lengths.

The test resonator was redesigned to meet the requirements mentioned in the previous section, and a complete analytical approach is given in Chap. IV. The outer conductor consists of a $\frac{3}{8}$" inside dia. copper tube, split into two lengths insulated from each other, as shown in the drawing, fig. 9, and the photographs, fig. 10 (left hand resonator) and 11. The sections are insulated by mica, and the flanges screwed together through insulating bushes. This enables current to be passed through the inner conductor without being by-passed by the outer conductor. The line is terminated at each end by a tight fitting copper plug, which has a $\lambda/4$ section, 0.1" dia. projecting from it. These plugs have holes drilled axially through them to allow the specimen, a 16 S.W.G. wire (.064" dia.) to be fitted. One of these plugs is/

is fixed and the other is adjusted so that the distance between them is one wavelength. Thus the specimen is $\lambda/2$ long and, since the supporting sections are $\lambda/4$ long, the junctions between them and the specimen carry little or no current and therefore poor contacts have a negligible effect on the Q of the resonator. For this reason also, the insulated junction in the outer conductor is made at the $\lambda/4$ point. All the internal surfaces were cleaned and polished as far as possible, to obtain a high Q. Three 5/16" dia. tubes, to allow coupling loops to be introduced, were placed at 120° intervals round one end. Another 5/16" dia. tube was placed, for the same reason, at the other end. This enables input and output loops to be placed far apart to minimise direct coupling.

Although, as will be described in a later paragraph, a standard resonator was found to be unnecessary, one was constructed for comparison purposes, and this is shown in the photograph, fig. 10 (right hand resonator). This is a $3\lambda/4$ resonator with a 0.1" dia. inner conductor, the input being fed to the $\lambda/2$ point and the crystal detector being coupled at the short-circuited end. The resonator may be tuned by a rod of polystyrene which can be screwed into the fringe field, at the open circuited end of the resonant line. Provision is also/

also made to allow the standard or the test resonator to be loaded. In place of the lossy line used by Milner and Clayton, a piece of carbon loaded dielectric was used. This was, in fact, part of a 100 ohm carbon resistor, rated at one watt. Other specimens of resistor were used, but all of them produced a progressive shift of the resonant frequency as they were introduced into the field due to the dielectric used as the resistor basis. Presumably the piece of resistor used was more heavily loaded with carbon as it produced a very small change in resonant frequency, which could be corrected by adjusting the klystron frequency.

In the method used in the experiments described in (a) and (b) of this chapter, the Q of the standard resonator was adjusted, by loading, to equal that of the test resonator. The height of the loaded Q curve could then be measured on the oscilloscope and compared to the height of the undamped curve. The measurement of these heights on an oscilloscope introduces parallax errors. One method of overcoming this is to use a calibrated Y-shift control. The following method, which was used, is more convenient.

Once balance has been obtained, the frequency modulating voltage is removed from the klystron and the output/

output of the standard resonator is disconnected from the oscilloscope and monitored by a microammeter. The reflector potential is then adjusted to give maximum output, i.e. the klystron is tuned to the resonant frequency of the resonator. The microammeter reading ($i_t$) is noted and the loading of the resonator removed. Due to the slight detuning caused by the dielectric of the load, a readjustment of the reflector voltage is necessary. Although this causes a slight error, as the klystron output changes when the reflector voltage is changed, it will not be greater than that introduced in the method described in (a) and (b) of this chapter. The new microammeter reading ($i_t$) is taken and the ratio $i_o/i_t$, which is the same as the ratio $h_o/h_t$ is used to calculate the Q ratio and hence the relative resistivity-oermeability product.

An important extension of the technique of Q measurement can be made, using the method of the last paragraph. Since the Q ratio can be measured by the height of the Q curve, the Q of the test resonator containing the specimen can be compared directly with the Q of the test resonator containing the reference specimen. From this, the skin effect relative to copper (the reference specimen) can be directly calculated without/

without the use of the standard resonator and the undesirable balancing. The objection to this method is that any drift in the klystron output introduces proportionate errors in the measurement of Q height. With reasonably simple precautions, however, this drift can be reduced so that the errors are less than those introduced by balancing; this is especially true at low Q where, as stated in (b), balancing was almost impossible.

The precautions taken were, that additional smoothing was used in the H.T. supply to the resonator, and H.T. batteries were used for the H.T. supply to the reflector, to reduce frequency modulation. When taking a long series of results, readings using the copper specimen were taken at regular intervals to check the reference standard. If this had drifted much, the intervening results were ignored.

Another advantage of this technique is the ease with which sudden changes of Q can be measured using an oscilloscope or pulse peak voltmeter. The oscilloscope method of measuring the change of permeability when pulsed or sinusoidal polarising fields are applied to the specimen is described in Chapters V and VI.

(d)/

(d) Calibration.

Considering eqn. 16, which will be proved in the next Chapter, it will be noted that the value of $\frac{k a_r}{\sqrt{\rho_r \mu_r}}$ is a constant decided by the reference specimen used and the resonator construction. The value of this constant is best obtained by experiment and to do this several different non-magnetic specimens of known resistivities were used. Each specimen was carefully cleaned, usually with nitric acid, and then the Q of the resonator using the specimen as inner conductor was compared with the Q using copper. For specimens of aluminium, molybdenum, brass, tantalum, eureka and brightray, the square root of the resistivity relative to copper was plotted to the inverse of the relative Q ratio, as shown in fig. 12. By eqn. 16 it is seen that for non-magnetic specimens of the same diameter as the copper specimen,

$$\sqrt{\frac{\rho_t}{\rho_r}} = \frac{Q_r}{Q_t}\left(\frac{k a_r}{\sqrt{\rho_r \mu_r}} + 1\right) - \frac{k a_r}{\sqrt{\rho_r \mu_r}}$$

i.e. a linear relationship. This is seen to agree, within experimental error, with the results in fig. 12, from which the constant $\frac{k a_r}{\sqrt{\rho_r \mu_r}}$ is found to be 17.3,

i.e.
$$\frac{a_r}{a_t}\sqrt{\frac{\rho_t \mu_t}{\rho_r \mu_r}} = 18.3\,\frac{Q_r}{Q_t} - 17.3 \quad -- (17)$$

$$= 18.3\sqrt{\frac{i_r}{i_t}} - 17.3 \quad --- (18)$$

## CHAPTER IV.

## DESIGN OF COAXIAL RESONATOR.

### (a) Theory of Coaxial Resonator.

It has already been stated in Chapter III that the type of resonator used by Milner and Clayton is unsuitable and that a resonator one wavelength long, fig. 9, was designed. The outline of this type of resonator is shown in fig. 13 where the specimen is of radius $a_1$, resistivity $\rho_1$, and permeability $\mu_1$; the rest of the resonator being constructed of a material of constants $\rho_2$ and $\mu_2$.

The Q of the resonator is then defined by the relation,

$$Q = 2\pi \frac{\text{energy stored per cycle}}{\text{energy dissipated per cycle}} \quad \text{---} \quad (19)$$

#### Stored Energy

The energy stored per cycle, $W' = \int \mu_o H^2 dV$.

Where H is the r.m.s. value of the field strength at any point in the resonator. Consider any small volume $\delta V$, situated at any point P; coordinates r, l and $\phi$.

In order to calculate the value of r.m.s. field strength, H, at P, let the value at point A (b, o, o) be $H_A$.

In the $\phi$ direction the field strength is constant;

in/

in the r direction it is inversely proportional to r; in the l direction, due to standing waves, a cosine variation occurs.

$$\text{i.e. } H = H_A \cdot \frac{b}{r} \cdot \cos \frac{2\pi l}{\lambda}$$

The volume in which the magnetic field exists is bounded by the metal surfaces. This can be divided into two volumes: that with outer dimension b, inner dimension $a_2$; and that with outer dimension b, inner dimension $a_1$. Since the integration is of $H^2$, it is immaterial whether H is positive or negative and thus integration from o to $\lambda/4$ added to integration from $3\lambda/4$ to $\lambda$ is equivalent to integration from o to $\lambda/2$. Similarly integration from $\lambda/4$ to $3\lambda/4$ can be replaced by integration from o to $\lambda/2$.

Then the stored energy per cycle is given by

$$W' = \int_{a_2}^{b}\int_{0}^{\lambda/2}\int_{0}^{360^\circ} \mu_0 H^2 r \, dr \, dl \, d\phi + \int_{a_1}^{b}\int_{0}^{\lambda/2}\int_{0}^{360^\circ} \mu_0 H^2 r \, dr \, dl \, d\phi$$

Since H is constant in the $\phi$ direction this can be rewritten,

$$W' = \int_{a_2}^{b}\int_{0}^{\lambda/2} \mu_0 H^2 2\pi r \, dr \, dl \, d\phi + \int_{a_1}^{b}\int_{0}^{\lambda/2} \mu_0 H^2 2\pi r \, dr \, dl \, d\phi$$

$$= \int_{0}^{\lambda/2} 2\pi b^2 \mu_0 H_A^2 \left(\cos \frac{2\pi l}{\lambda}\right) \log_e \frac{b}{a} \, dl + \int_{0}^{\lambda/2} 2\pi b^2 \mu_0 H_A^2 \left(\cos \frac{2\pi l}{\lambda}\right)^2 \log_e \frac{b}{a_2} \, dl$$

$$= \pi b^2 \mu_0 H_A^2 \log_e \left(\frac{b^2}{a_1 a_2}\right) \cdot \frac{\lambda}{2} \qquad \text{— (20)}$$

Energy Loss per Cycle.

Since the dielectric in the resonator is air, the dielectric loss can be ignored. The only loss is therefore dissipation in the metal walls. A convenient equation for this form of loss is given by Barlow and Cullen[22], although similar equations will be found in other standard works. The equation is

$$W_m = 2\pi\sqrt{\frac{2\rho}{\omega\,\mu_o\,\mu_m}}\iint \tfrac{1}{2}\mu_o\mu_m H_s^2\, dS.$$

where Wm is the energy dissipated in a surface, S, of metal, resistivity $\rho$, permeability $\mu_m$, the r.m.s field strength in the surface being $H_S$.

This equation may be more conveniently written

$$W_m = \sqrt{\pi\rho\mu_o\mu_m/f}\iint H_s^2\, dS.$$

In order to apply this equation, it is necessary to divide the surface into sections and integrate, as follows:-

1. Loss in End Plates.

$r = a_2$ to $b$; $l = 0$ and $\lambda$; $\phi = 0$ to $360°$.

Metal constants $\rho_2$ and $\mu_2$.

Consider the loss in a ring of area $2\pi r\, dr$.

The loss in the two end plates can be written as

$$W_1 = 2\sqrt{\pi\rho_2\mu_o\mu_2/f}\int_{a_2}^{b} H_A^2 \cdot \frac{b^2}{r^2} \cdot 2\pi r\, dr.$$

$$\frac{\pi}{2} b^2 H_A^2 \sqrt{\pi\mu_o/f}\left(8\sqrt{\rho_2\mu_2}\log_e\frac{b}{a_2}\right)$$

There are similar sections at $l = \frac{\lambda}{4}$ and $\frac{3\lambda}{4}$ but no loss occurs since H = 0 at these points.

2. Loss in Cylindrical Outer Conductor.

$r = b$ ; $l = 0$ to $\lambda$ ; $\phi = 0$ to $360°$

Metal constants $\rho_2$ and $\mu_2$

The integral from 0 to $\lambda$ is equivalent to twice the integral from 0 to $\frac{\lambda}{2}$ .

$$W_2 = 2\sqrt{\pi \rho_2 \mu_2 \mu_0 / f} \int_0^{\lambda/2} H_A^2 \left(\cos \frac{2\pi l}{\lambda}\right)^2 2\pi b \, dl$$

$$= \frac{\pi}{2} b^2 H_A^2 \sqrt{\pi \mu_0 / f} \left(\frac{2\lambda}{b} \sqrt{\rho_2 \mu_2}\right)$$

3. Losses in Part of Inner Conductor.

$r = a_2$ ; $l = 0$ to $\frac{\lambda}{4}$ and $\frac{3\lambda}{4}$ to $\lambda$ ; $\phi = 0$ to $360°$.

Metal constants $\rho_2$ and $\mu_2$.

Since the integration is of $H^2$, it is immaterial whether H is positive or negative and the integration with respect to l can be carried out over the range 0 to $\frac{\lambda}{2}$

Hence, $W_3 = \frac{\pi}{2} b^2 H_A^2 \sqrt{\pi \mu_0 / f} \left(\frac{\lambda}{a_2} \sqrt{\rho_2 \mu_2}\right)$.

4. Losses in Remainder of Inner Conductor.

$r = a_1$ ; $l = \frac{\lambda}{4}$ to $\frac{3\lambda}{4}$ ; $\phi = 0$ to $360°$.

Metal constants $\rho_1$ and $u_1$.

This integration may also be carried out between 0 and $\frac{\lambda}{2}$

Hence, $W_4 = \frac{\pi}{2} b^2 H_A^2 \sqrt{\pi \mu_0 / f} \left(\frac{\lambda}{a_1} \sqrt{\rho_1 \mu_1}\right)$.

Therefore the total energy loss in the resonator is

$$W_m = W_1 + W_2 + W_3 + W_4$$

$$= \frac{\pi}{2} b^2 H_A^2 \sqrt{\pi \mu_0 / f} \left(8\sqrt{\rho_2 \mu_2} \log_e \frac{b}{a_2} + 2\frac{\lambda}{b}\sqrt{\rho_2 \mu_2} + \frac{\lambda}{a_2}\sqrt{\rho_2 \mu_2} + \frac{\lambda}{a_1}\sqrt{\rho_1 \mu_1}\right) \quad \text{—— (21)}$$

Hence, from eqns. 19, 20 and 21,

$$Q = 2\pi \frac{\pi b^2 H_A^2 \mu_0 \left(\log_e \frac{b^2}{a_1 a_2}\right) \cdot \frac{\lambda}{2}}{\frac{\pi}{2} b^2 H_A^2 \sqrt{\pi \mu_0 / f} \left(8\sqrt{\rho_2 \mu_2} \log_e \frac{b}{a_2} + 2\frac{\lambda}{b}\sqrt{\rho_2 \mu_2} + \frac{\lambda}{a_2}\sqrt{\rho_2 \mu_2} + \frac{\lambda}{a_1}\sqrt{\rho_1 \mu_1}\right)}$$

$$= \frac{2\sqrt{\pi f \mu_0} \log_e \frac{b^2}{a_1 a_2}}{\frac{8}{\lambda}\sqrt{\rho_2 \mu_2} \log_e \frac{b}{a_2} + \frac{2}{b}\sqrt{\rho_2 \mu_2} + \frac{1}{a_2}\sqrt{\rho_2 \mu_2} + \frac{1}{a_1}\sqrt{\rho_1 \mu_1}} \quad \text{—— (22)}$$

Conditions for Maximum Q.

Theoretical methods of determination of maximum Q were found to be too involved and therefore a graphical solution had to be employed. In order to simplify computation, it was decided to study the value of the function

$$F = \frac{\log_e \left(\frac{b}{a_1} \cdot \frac{b}{a_2}\right)}{8\frac{b}{\lambda} \log_e \frac{b}{a_2} + 2 + \frac{b}{a_2} + \frac{b}{a_1}\sqrt{\frac{\rho_1 \mu_1}{\rho_2 \mu_2}}}$$

i.e. $$Q = 2b\sqrt{\frac{\pi f \mu_0}{\mu_2 \rho_2}} \times F$$

Curves of the value of F were drawn for different values/

values of $\frac{b}{a_1}$, $\frac{b}{a_2}$ and $\sqrt{\frac{\rho_1 \mu_1}{\rho_2 \mu_2}}$. With the resonator constructed entirely of one material it was found that F reached a maximum for $\frac{b}{a_1} = \frac{b}{a_2} = 3.6$. This agrees with the well known solution[23,24] for a coaxial resonator with a constant diameter inner conductor. If the resonator is constructed of two different materials the maximum Q does not occur when the ratio of outer conductor radius to inner conductor radius is the same for each section. For example if the resonator is of copper and the specimen is brass, the maximum Q occurs when the ratios are 2.5 and 6 respectively.

For the present application it is desirable to make the Q a maximum with copper specimen, in a copper resonator. It is obvious that in the suggested construction, $a_2$ cannot be made equal to $a_1$ but, fortunately, it is found that the curve of Q, with respect to radius ratios, is fairly flat near the optimum value. The outer conductor was therefore made of $\frac{3}{8}$" inside diameter copper tube; the inner was made 0.1" diameter, being turned integral with the end plug; with a specimen of 16 S.W.G. (.064" dia.) wire. This departure from optimum conditions causes less than 3% drop in Q. The theoretical maximum Q is 8,030, but, unfortunately, there was no means of checking the absolute value experimentally.

A/

A drawing and photographs of the resonator are given in figs. 9, 10 and 11.

(b) Relation between Q and Specimen Characteristics.

In eqn. 22 the first three terms of the denominator are seen to be a constant of the resonator and can therefore be replaced by a constant k. Then, the equation becomes

$$Q = \frac{2\sqrt{\pi f \mu_0}\log_e \frac{b^2}{a_1 a_2}}{k + \frac{1}{a_1}\sqrt{\rho_1 \mu_1}}$$

Consider, first, the resonator with a reference specimen as inner conductor and, using a subscript r to denote the symbols referring to it,

$$\text{Then } Q_r = \frac{2\sqrt{\pi f \mu_0}\log_e \frac{b^2}{a_r a_2}}{k + \frac{1}{a_r}\sqrt{\rho_r \mu_r}} \qquad \text{— (23)}$$

If, now, the reference specimen is replaced by a test specimen, subscript t,

$$\text{Then } Q_t = \frac{2\sqrt{\pi f \mu_0}\log_e \frac{b^2}{a_t a_2}}{k + \frac{1}{a_t}\sqrt{\rho_t \mu_t}} \qquad \text{— (24)}$$

Dividing eqn. 23 by eqn. 24,

$$\frac{Q_r}{Q_t} = \frac{\log_e \frac{b^2}{a_r a_2}}{\log_e \frac{b^2}{a_t a_2}} \times \frac{k + \frac{1}{a_t}\sqrt{\rho_t \mu_t}}{k + \frac{1}{a_r}\sqrt{\rho_r \mu_r}}$$

The factor $\frac{\log_e \frac{b^2}{a_r a_2}}{\log_e \frac{b^2}{a_t a_2}}$ was not included in the equation quoted/

quoted by Milner and Clayton[19], but, for reference and test specimens of approximately equal diameters, the error is unimportant. For example in the resonator described above, a change of ±3.2% in specimen diameter causes only a ±1% variation in Q ratio. Thus, provided the test specimen diameter is not greatly different from that of the reference specimen,

$$\frac{Q_r}{Q_t} = \frac{k + \frac{1}{a}\sqrt{\rho_t \mu_t}}{k + \frac{1}{a}\sqrt{\rho_r \mu_r}}$$

which can be rearranged to give eqn. 16.

(c) The Relation between Measured Crystal Current and Q.

The equivalent circuit of the coaxial resonator can be simplified to that shown in fig. 14(a). This differs from the usual equivalent circuit[25] which shows many coupled, tuned circuits and has coupling between input and output loops. The simplification to a single tuned circuit is permissable since the resonator is only being considered around one resonance peak, that is, in one mode. The coupling between input and detector loops can be ignored since, as was stated in Chapter III, this coupling was reduced to negligible proportions.

As both input and output couplings are of low value, two/

two further simplifications can be made to this circuit: firstly, it can be assumed that the electric field injected into the resonator is constant since, due to the low coupling, changes in the resonator are not reflected back to the supply; in the circuit diagram, this is equivalent to a constant voltage supply to the tuned circuit, fig.14(b). Secondly, the detector loop acts as a current transformer because of the low impedance of the crystal circuit. Due to the characteristics of the crystal, the current in the equivalent circuit is proportional to the square root of the crystal current, $i_c$.

If the circuit of fig.14(b) is supplied at a constant voltage V, at its resonant angular frequency, w, then $\sqrt{i_c} \propto I = \frac{V}{R} = \frac{V}{\omega L} \times \frac{\omega L}{R} = \text{a constant} \times Q$

$$\text{i.e. } Q \propto \sqrt{i_c}$$

If, with the reference specimen in the resonator, the peak crystal current is $i_r$, and with the test specimen it is $i_t$,

$$\text{then } \frac{Q_r}{Q_t} = \sqrt{\frac{i_r}{i_t}} \qquad \text{— (25)}$$

The accuracy of this relationship depends on the input from the klystron remaining constant. The practical precautions taken have already been discussed in Chapter III.

Eqns./

Eqns. 17 and 25 can then be combined to give the equation which enables the calculation of the product of resistivity and permeability, of the test specimen, to be made from measurements of crystal current. This is eqn. 18 which has already been given at the end of Chapter III.

## CHAPTER V.

## SEPARATION OF RESISTIVITY AND PERMEABILITY AT MICROWAVES.

### (a) Choice of Method.

The measurement of the Q of the resonator, containing the specimen, relative to the Q, containing a copper conductor has already been described in Chapter III (c). Using eqn.18 the product of resistivity and permeability can be calculated for the specimen. To obtain the value of permeability alone, requires either: that the resistivity of the specimen at microwave frequencies is assumed equal to its d.c. value; or that the resistivity of the specimen is measured independently of the permeability. Obviously it is advantageous to use the second, more difficult, alternative since, as has already been mentioned in Chapter II, the scratching, etc. of the surface of the specimen can produce wide variations of resistivity. This can be appreciated from a calculation of the skin depth at the frequency used ($3,000^{Mc}/s$). If the specimen has a product of ($\rho\mu$) of 100, relative to copper, the skin depth is only $1.2 \times 10^{-4}$mm. Small perturbations on the surface can therefore have a profound effect on the apparent resistivity.

Before considering the more difficult method, the author/

author looked into methods of electro polishing the specimen in order to reduce errors from this source. It was found that the polishing of iron and steel wires is a difficult operation, not likely to produce dependable results. Parcel[26] has described a technique of polishing small, flat, steel specimens. It appears that the results were not very dependable and the application to wires would introduce further complications; for example it would be difficult to ensure regular polishing all round the wire, even if a coaxial cylinder were used as a cathode.

The other alternative, the independent measurement of resistivity, was therefore pursued and it appears that no method exists whereby a measurement of either resistivity or permeability alone can be made at high frequencies. The only methods of measuring resistivity and permeability at high frequencies are:

(1) The measurement of the wavelength in a coaxial line or a waveguide.

(2) The measurement of the loss in a coaxial line or a waveguide, whether by measuring attenuation or Q.

Both of these methods result in a value for the product of the resistivity ($\rho$) and the permeability ($\mu_L$ or $\mu_R$) of/

of the specimen. Thus, the only way of measuring the resistivity is to reduce the permeability to unity.

The work of Millership and Webster[7] has shown that, beyond about 1500 $^{Mc}/_{s}$, the inductive permeability ($\mu_L$) is unity for all the materials used by them. The difficulty of applying their technique at higher frequencies is that, in order to produce a measurable difference between the wavelength in the guide and that in free space, the specimen must be an exceedingly fine wire.

It was therefore decided to employ an alternative technique, used by Johnson and Rado[20], in which the resistive permeability ($\mu_R$) is reduced to unity by the application of a saturating field, parallel to the high frequency magnetic field. Since, in the coaxial resonator used, the field traverses the wire in concentric circles, the saturating field must be applied by passing a high current through the wire, in a longitudinal direction. This results in difficulties due to heating which will be described in section (d) and experiments at low polarising fields will now be discussed.

(b) Measurements at Low Polarising Fields.

It has already been mentioned (Chapter IV) that the/

the outer conductor of the resonator has been constructed in two sections which are insulated from each other to enable a current to be passed through the specimen (cf. fig. 16(a)). If this current has a value $I_p$, the polarising field has a maximum value

$$\hat{H}_p = \frac{I_p}{\pi 2 a_t} \qquad -(26)$$

where $a_t$ is the radius of the test specimen in metres. This maximum value is reached at the surface of the specimen. Since the penetration depth of the microwave field is extremely small, this is the field strength which affects the parameters of the specimen in the microwave field.

If the peak crystal current of the resonator output is i when no polarising field is applied, and $i_p$ when $\hat{H}_p$ is applied; and the permeability changes from $\mu$ to $\mu_p$, the resistivity remaining constant: then eqn. 18 becomes

$$\sqrt{\frac{\mu}{\mu_p}} = 18{\cdot}3 \sqrt{\frac{i_p}{i}} - 17{\cdot}3 .$$

In practice this can be carried out in the same way as the measurements described in Chapter III(c). The crystal current (i) is measured without polarising current and then a steady current of $I_p$ is passed through the specimen to produce/

produce a field $\hat{H}_p$. The new steady value of the crystal current, $i_p$, can then be measured. This is a reasonable method for currents up to 10A, above which value the heating of the 16 S.W.G. centre conductor becomes excessive and precludes the use of a steady current. Before discussing how this is overcome, the types of curves taken with currents up to 10A will be discussed.

(c) Butterfly Curves.

If the polarising field applied to the specimen is varied cyclically between $+H_2$ and $-H_2$ and the permeability is measured at points throughout the cycle, a curve of permeability to a base of polarising field can be drawn out as shown in fig.15(a). Curves of this type were taken by Johnson and Rado[20] and were called "butterfly" curves.

At first the similarity between this curve and the B-H loop, fig. 15(b), is not apparent. When it is realised that in fig.15(a) the permeability is incremental (since it is measured by means of an alternating, high frequency, field superimposed on a d.c. field) it will also be realised that fig.15(a) must be the graph of the slope of fig.15(b). This is borne out by the following points.

(1) The maximum values of the slope in fig. 15(b) occur at the points of inflexion, when the curve crosses the

H/

H-axis at $+H_1$ and $-H_1$ and correspond to the peaks of permeability, value $\mu_1$, in fig.15(a).

(2) The minimum values of slope and permeability ($\mu_2$) occur at the maximum values of field strength $+H_2$ and $-H_2$, i.e. nearest to saturation.

(3) Due to the symmetry of the B-H curve, the cross-over of the butterfly curve occurs at H = 0, when the permeability is $\mu_3$.

In this way the connection between the butterfly curve and the hysteresis loop can be appreciated. Since the hysteresis loop can only be taken using d.c. or by integrating a butterfly curve, the butterfly curve becomes very important in alternating current measurements.

(d) Saturation Value of Polarising Field.

The methods of measurement at microwave frequencies described in this Chapter have been made without, or with low, polarising fields. The most valuable measurement, however, is that made when the specimen is saturated, i.e. the permeability is unity. By this means the resistivity of the specumen can be found and the permeability of the unpolarised material calculated. Unfortunately, in most cases/

cases, it is not possible to saturate the material, even with the pulse method to be described, due to the very high current required and the measurements have to be made at several high values and extrapolated to saturation.

It has already been mentioned that heating precludes the measurement of permeability for polarising currents of over 10 A. Therefore the current must be applied as a short pulse, preventing the use of a meter to measure the change in Q of the resonator.

A method using a single pulse peak voltmeter to measure the peak pulse output of the resonator has been described by Johnson and Rado[20] and Rado et al[27]. This is an accurate method of measurement, but it requires careful calibration and well regulated power supplies. Although it would be desirable to build such a unit if a long series of measurements were contemplated, the author felt that it would be preferable to devise a method using standard equipment. This led to the development of the following oscillographic method.

The output of the crystal detector is connected, fig.16(a), to the A1 amplifier of a Cossor 1039 oscillograph and the trigger circuit connected as shown. For the time being/

being, the A2 connection can be ignored. When the switch (a two pole heavy duty knife switch) is closed, a pulse of current is passed through the specimen and, at the same time, the time base is triggered. This results in a pulsed change of output as shown in fig.16(b), which shows the A1 and A2 traces on the oscillograph. The height of the A1 pulse is proportional to the change in crystal current. The shape of the curve is largely dependent on the amplifier characteristics and cannot be used to comment on the pulse properties of the magnetic specimen, with respect to time. In order to measure the polarising current, a resistor $R_s$ is connected in series with the specimen and the voltage across it is applied to the A2 plates, resulting in a deflection similar to the A1 deflection, as shown in fig.16 (b).

In order to calibrate the A1 amplifier, the apparatus was set up as shown in fig.16(c). With switch S1 in position 2, the microammeter was set to a suitable reading by loading the Q of the test resonator. With switch S1 returned to position 1 and the camera shutter opened, S2 was switched from position 2 to 1, i.e. from earth to the voltage output of the detector. This was repeated for a series/

series of current values and trace height plotted against microammeter reading. This curve was found to be linear below the overloading limit of the amplifier.

It will be realised that this method introduces several errors caused as follows:

(a) A change in the mains voltage causes a variation in the HT voltage of the oscillograph amplifier and the deflection will therefore not obey the calibration curve.

(b) Drift of the klystron output causes changes in the initial reading of crystal current.

(c) Processing of the photographic material causes stretching which will vary from time to time.

The following precautions were taken to reduce errors due to these causes:

(1) The mains voltage was set, if necessary, before each reading, by means of a variable transformer and a voltmeter. This was found to be sufficient to overcome (a) as the deflection was not particularly sensitive to mains fluctuations.

(2) The crystal current output of the resonator with copper inner conductor was checked before and after each series of readings. This provided a check on/

on errors due to (b).

(3) At the start and finish of each series of photographs several A1 calibration points were taken and used to draw a calibration curve from which the other readings were calculated. This reduced errors due to (c).

The value of the polarising current must also be measured and, as has already been mentioned, the voltage across $R_s$, fig. 16(a) is therefore applied to the A2 amplifier. The deflection produced must then be related to the current passing through the specimen, and this calibration is carried out using the circuit of fig.17(a).

Steady currents of up to 100A were passed through the circuit, by closing S1 fig.17(a), and the ammeter reading noted. S1 was then opened and the camera shutter opened. S1 was then closed and then the shutter closed, giving a photograph of the A2 deflection (on a triggered time base). The ammeter was set to various current values, by varying the amount of resistance wire in circuit, and a series of results taken, enabling a calibration curve to be plotted.

It was found convenient, for check purposes, to make/

make a calibration curve of deflection against voltage input, using the circuit of figure 17(b). The A2 amplifier was not often checked as accuracy in current measurement was not of prime importance. By relating this curve to the above curve $R_s$ was found to be .038 ohms. which agreed with a measured value, using d.c.

(e) Example of Measurement and Calculation.

The method employed in these measurements can best be described by means of an example, and, as the results for annealed nickel show saturation, they will be used. Firstly, calibration curves of the A1 amplifier for both the 150 and 500 mV ranges were constructed. These were straight lines passing through the following points: 150 mV scale; $i_c = 2$, deflection = 0.25 in.on photographic paper, and $i_c = 4$ deflection = 0.51 in.
(Note: the crystal currents are purely arbitrary as a galvanometer marked in scale divisions was used.)
500 mV scale; $i_c = 3$, deflection = 0.13 in. and $i_c = 7$, deflection = 0.3 in.

The A2 calibration was a straight line passing through V = 1.4V, deflection = 0.14 in. and V = 5.3V., deflection = 0.51" for the 5 volt range. The corresponding graph/

graph for the 15V scale is slightly curved and will not be detailed.

First of all with a copper inner conductor in the resonator the crystal current was found to be 13.9. The nickel specimen was then used as inner conductor and the peak crystal current found to be 6.7. The results of the various readings taken with polarising currents are given in Table II. It will be noted that before each photograph, the crystal current without polarising field was taken (column 4).

Column 1 shows the nominal voltage of the accumulator supplying current to the specimen. Columns 2 and 3 are the deflections measured on the photographic paper for the A1 and A2 amplifier respectively. Column 5 is the change in crystal current, calculated from column 2 by means of the calibration curve. Column 5 is then added to column 4 to give the peak value (x) reached by the crystal current. This is then used to calculate the Q ratio of the polarised specimen to copper (Column 7). Using eqn. 18, the value of $(\sqrt{\rho\mu}\ )_{rel.}$ and hence $\rho\mu$ relative to copper is calculated (column 8).

The value of $\hat{H}_p$ corresponding to each reading

is/

## TABLE II

With copper as standrad, $i_c = 13.9$

| Col. No. 1 | 2 | 3 | 4 | 5 | 6 | 7 | 8 | 9 | 10 |
|---|---|---|---|---|---|---|---|---|---|
| Applied Voltage | A1 Deflection | A2 Deflection | $i_o$ | Change in crystal current | x | Q ratio $=\sqrt{\frac{13.9}{x}}$ | $\rho\mu$ | $V_{shunt}$ | $\hat{H}$ |
| 0 | 150 m v scale | 5 v scale | 6.7 | 0 | 6.7 | 1.44 | 83 | 0 | 0 |
| 6 | 0.21 | 0.24 | 6.8 | 1.7 | 8.5 | 1.28 | 37 | 2.4 | 12.5 x $10^3$ |
| 12 | 0.50 | 0.43 | 6.8 | | | | | | |
| 12 | 50 m v scale | | | 3.9 | 10.7 | 1.14 | 13 | 4.4 | 22.6 |
| | 0.17 | 0.43 | 6.8 | | | | | | |
| 24 | 0.19 | 15 v scale 0.26 | 6.8 | 4.5 | 11.3 | 1.11 | 9 | 9.9 | 50.9 |
| 36 | 0.19 | 0.30 | 7.0 | | | | | | |
| | | | | 4.5 | 11.5 | 1.10 | 8.7 | 10.5 | 55 |
| 48 | 0.19 | 0.30 | 7.0 | | | | | Amplifier Saturated. | |

54A

is calculated as follows: Using the calibration curve of the A2 amplifiers, the voltage across $R_s$ (.058 ohms.) is calculated (column 9). The polarising field on the surface of the conductor can then be calculated from eqn. 26 as follows:

$$\hat{H}_p = \frac{I}{2\pi a_t} = \frac{V}{R_s 2\pi a_t} = 5{\cdot}14\times10^3 . V \ A/m$$

This enables column 10 to be calculated.

The relation between $\rho\mu$ and H given in Table II is illustrated in fig. 32. Higher values of field strength have been omitted from the curve, but it will be noted that little change in the permeability occurs beyond the points shown.

CHAPTER VI.

## Microwave Butterfly Curves using A.C. Polarising Field: Circular and Longitudinal Fields.

### (a) Circular Fields.

The drawing out of butterfly curves by a point-by-point method has been described in the previous chapter. Little of quantitative value can be derived from these curves and it is therefore sufficient if the shape of the curve is delineated by an oscillographic method, as follows.

An alternating current is passed through the specimen by a transformer connected to terminals AA (fig. 18). This transformer is fed from the 250 V 50 $^{c}/_{s}$ supply through variac (auto transformer with continuously variable tap) by which means the current in the specimen may be set to a suitable/

suitable value. The detected output of the resonator then varies in proportion to the a.c. polarising field. This is fed to the A1 amplifiers of a Cossor 1039 oscillograph, producing a deflection on the tube. In order to present this as a butterfly curve, the time base must be in step with the variations in the applied field. Another transformer and variac are therefore used to supply a sinusoidal time base. Approximately the same phase changes occur in the time base circuit as in the polarising circuit, therefore the two signals are almost in phase. This was checked with the A2 plates connected as shown in fig. 18, producing very little departure from a straight line.

Fig. 19 (a) to (f) is a set of photographs taken, for different peak values of circular polarising field, on a specimen of strand annealed mumetal (i.e. annealed in coils, before leaving the factory: a certain amount of strain is incurred by the working necessary to straighten the specimen). As would be expected, as the peak field increases, the permeability variation also increases.

The time base width was maintained constant throughout these photographs: it might have been preferable to/

to make the length of time base proportional to the applied field, thus the scale of the photographs would be accurate; however, as some photographs required a change of amplification of the detected signal, it would be difficult to maintain constant scale throughout. Between (d) and (e) the meter registering the current in the specimen, was changed, resulting in a slightly different phase shift and a correspondingly altered curve.

Photographs 19 (g) to (j) show similar curves for an annealed specimen of mumetal. The method of annealing is described in Chapter IX.

(b) Longitudinal Fields.

If a longitudinal alternating field is now applied to the specimen, through terminals BB, fig. 18, butterfly curves can again be obtained (e.g. fig. 20 (f)). The winding which produces the longitudinal field consists of 3 layers, each of 30 turnsof flexible, plastic covered wire. Unfortunately the flanges joining the two parts of the resonator prevented this winding projecting beyond the ends of the $\lambda/2$ section of specimen, which would have ensured a homogeneous field.

Figure/

Figure 20 (a) to (g) shows a series of photographs with varying peak longitudinal field taken on a specimen of strand annealed mumental. The first two curves, (a) and (b) show very marked asymmetry due to the effect of the earths vertical field (approx 24 A/m). From the photographs it appears that the longitudinal field causes a reduction rather than an increase in Q at peak field strength. Tests carried out using a d.c. field showed this to be the case. Further results of this effect will be given in Chapter IX.

(c) Combined Circular and Longitudinal Fields.

Since the effect of a circular polarising field is to increase Q while that of a longitudinal field is to decrease Q it is interesting to study the effect of these fields in combination.

Figure 21 shows the effect, on a mumetal specimen, of a d.c. longitudinal field superimposed on an a.c. circular field. In (a) only the circular field is applied, while (b) and (c) show the effect of a superimposed d.c. longitudinal field. It will be seen that the amplitude of the butterfly curve is reduced by the applied field, in fact other measurements/

measurements showed that the curve had degenerated to a straight line when a d.c. longitudinal field equal to the peak circular field was applied.

Photographs (d) to (f) show the effect of reversing the superimposed field and it is seen that the effect is similar regardless of direction. Naturally a slight difference exists due to the presence of the earth's vertical field.

If, now, an a.c. longitudinal field is applied giving a butterfly curve, fig 22 (a) and (b), the effect of an additional d.c. circular field is to increase the amplitude of the curve, fig 22 (c) and (d) and to alter the shape considerably. This applied circular field requires to be large with respect to the peak longitudinal field to produce a noticeable change.

Further results of measurements on various specimens using this technique will be given in Chapter IX.

(d) Calculation, from Photographs, of Change of Product ($\rho\mu$) during Butterfly Curve.

The photographs which have been described give no direct indication of the change of the product ($\rho\mu$) that occurs/

occurs during the cycle. When only one type of specimen is being considered, the relative changes can be compared from photograph to photograph. If different specimens are being employed, however, it is necessary to be able to calculate these changes as the scale of the curve is different for different initial values of $(\rho\mu)$. The height of the butterfly curve can be measured and $\delta i$, the change in crystal current, calculated. This change must be related to a known point on the curve before the change in $(\rho\mu)$ can be calculated.

From butterfly curves of strand annealed mumetal, using a circular field and the point by point method described in Chapter V, it was found that the following assumption could be made: the peak value of $(\rho\mu)$ is approximately that of the specimen with no applied field. Using this assumption, if $i_o$ is the peak crystal current of the resonator with a copper inner and $i$ is the crystal current with a specimen of relative product of resistivity and permeability, $(\rho\mu)$, then

$$(\rho\mu) \propto \frac{i_o}{i}$$

If/

If $di_1$ is the change in crystal current measured from the photograph, then the minimum value $(\rho\mu)_1$, is given by

$$(\rho\mu)_1 \propto \frac{i_o}{i+\delta i_1}$$

and hence $\delta(\rho\mu) = (\rho\mu) - (\rho\mu_1)$ can be calculated.

When a cyclic longitudinal field is applied to the specimen it is found that the initial value of the product $(\rho\mu)$ corresponds to the minimum of the butterfly curve, i.e. if $\delta i_2$ is the measured change in crystal current, then the maximum value,

$$(\rho\mu)_2 \propto \frac{i_o}{i-\delta i_2}$$

and hence the change in $(\rho\mu)$ can be calculated.

The case of combined fields is a little more complicated. When a d.c. longitudinal field is superimposed on an a.c. circular field, the butterfly curve tends to drop to zero. There is little point in calculating these changes and therefore no method was developed.

When a d.c. circular field is superimposed on an a.c. longitudinal field, an increase in the overall height of the butterfly curve occurs. To study this effect, the most suitable example in figure 37 (b) and (c) which shows the effect (b) of a longitudinal field with (c) a superimposed circular/

circular field. There it can be seen, and this is confirmed by point by point measurements, that the dips of the curve (b) deepen downwards in (c) while the level of the top remains approximately constant. If $di_3$ is the change of crystal current, then

$$(\rho\mu)_{3min} \propto \frac{i_0}{i+(\delta i_3 - \delta i_2)} \text{ and } (\rho\mu)_{3max} \propto \frac{i_0}{i-\delta i_2}$$

from which $\delta(\rho\mu)_3$ can be calculated.

These methods were used to calculate the values given in figs 33-43.

## CHAPTER VII

## PERMEABILITY MEASUREMENTS USING D.C. or Low Frequency Fields.

### (a) General Considerations

The initial permeability has been defined in Chapter I as the static permeability when the applied field strength tends to zero. Since the permeability remains fairly constant if d.c. or low frequency fields up to several kilocycles are used, these measurements can be made using an a.c. field. Where possible, the author felt that an a.c. measurement should be avoided and preference given to a d.c. measurement, even if only from the purist attitude that it is the method which conforms to the definition of static field. Other factors help in this decision: the d.c. method is not troubled by harmonics in the a.c. supply; nor is a stable frequency required. It must be noted, however, that the author was driven to the use of alternating fields in order to be able to measure circular permeability, as described in section (d).

The best known methods of measuring the permeability of a wire or rod specimen use a longitudinal applied field, and it is such a method that the author used at first. The methods considered and the one used, are described in section (b

While/

While carrying out measurements at high frequencies using the polarising technique described in Chapter V, the author realised that, since the high frequency field is applied to the specimen in a circular direction, it would be preferable if the static permeability could be measured in a similar way. Attempts were made to repeat several methods described in various articles. These attempts, none of which produced satisfactory results, are described in section (c) and in section (d) a method is described which was developed by the author.

(b) Longitudinal Permeability.

The first method considered, was that used by Hodsman et al[21] in which the specimen, a wire, is used as the core of a mutual inductance of solenoid form. Using a 500$^{c}$/s Hartshorn bridge, the values of mutual inductance with and without the specimen are compared, and the inductive permeability calculated. This method, since it employs a.c. was not used for the reasons mentioned in (a). The second alternative was that used by Johnson and Rado[20] in which a short rod specimen was employed. The magnetising field

was/

was applied by a solenoid and the flux change was measured ballistically. The disadvantage of this method is that a correction has to be applied because of the low ratio of length to diameter of the specimen. It is very difficult to apply accurate correction for rod specimens and the field distortion at the ends of the specimen can cause serious errors. Thirdly, the method used by Kreidsheimer[2] was considered. In this the magnetic wire specimen is wound to form a ring shape. A magnetising coil is then wound on to the ring, forming a toroid. A search coil is wound over the toroid and ballistic measurements carried out. The disadvantage of this method is that stresses are set up when winding the specimen into ring form, causing an alteration in the magnetic properties.

The following method which was used by Ewing and, later, by Cioffi,[28] was found to be suitable and was adopted by the author. It was a straight forward ballistic method in which the specimen was at the centre of a long solenoid with a short, many turned, search coil inside the solenoid. It has already been mentioned that Ewing found, experimentally, that a specimen at least 300 diameters long could be considered/

considered infinite. The magnetising solenoid consisted of a 20 SWG winding on a ½ in. inside dia. former 2 ft. 6 in. long, i.e. 470 times the specimen diameter (.064 in.). The 20,000 turn search coil was wound on a glass tube 0.2 in. dia. with resin bonded fibre end checks which were ½ in. dia. to give a sliding fit inside the solenoid. Each end cheek had a hole drilled axially through it to hold the 16 SWG specimen along the central axis of the search coil and solenoid. At each end of the magnetising solenoid, tightly fitting end plugs, similar to the cheeks on the search coil, held the specimen central.

The apparatus was then connected into the circuit shown in Figure 23 where it will be noted that there were two magnetising solenoids on the former. These were wound, one on top of the other, of 20 S.W.G. enamelled wire close wound (26 T.P.I.). The first was used to apply the reversible field, the second to apply a polarising field. With the specimen in position, and a set value of polarising field, the current in the first solenoid was reversed and the deflection of the ballistic galvanometer noted. This was repeated/

repeated without a magnetic inner wire. The two results obtained were used to calculate the permeability of the wire.

Before use, the apparatus required to be calibrated; as the method is well known, the calculations will not be given in detail and a purely descriptive outline will be given.

The equipment used consisted of a standard solenoid (N.P.L. certificated), search coil and a F.G. ammeter. The standard search coil was connected in series with the test search coil, damping resistor and the ballistic galvanometer: these items remained in circuit throughout the readings so that the resistance of the galvanometer circuit was not altered. The following measurements were then made:-

(1) A measured current was reversed in the standard solenoid, containing its own search coil, and the ballistic deflection noted.

(2) The standard search coil was now replaced by the test search coil. This had special circular wooden end cheeks to centralise it, axially, in the standard solenoid. A measured current in the standard solenoid is then reversed and the galvanometer deflection noted.

(3)/

(3) With the test search coil in the test solenoid, a known current was reversed in the first test solenoid and the galvanometer deflection noted.

(4) Part (3) was repeated for the second test solenoid.

Using (1) the galvanometer constant $k_g$ . can be calculated. From (2) the area turns of the test search coil can be found. From (3) and (4) the magnetising force per amp can be calculated for each test solenoid.

Using the constants found above, the permeability of a specimen can then be calculated as follows:-

If a current $I_1$, producing a field of strength $H_1$, is reversed in the magnetising solenoid, and a deflection $\theta_1$ is produced, when there is no specimen; and, when a current $I_2$, producing a field of strength $H_2$, is reversed there is a deflection $\theta_2$ with a specimen of permeability $\mu$ and if a is the cross-sectional area of the specimen and A the mean cross sectional area of the search coil of turns and $k_g$ the galvanometer constant,

then $$\theta_1 = k_g 2H_1 AT \quad \text{---------} \quad (27)$$

and $$\theta_2 = k_g 2H_2 \{AT - aT + \mu aT\} \quad \text{- - - -} \quad (28)$$

Dividing (27) by (28) and simplifying, noting that $H_1/H_2 = I_1/I_2$

$$\mu = \frac{A}{a}\left\{\frac{I_1\theta_2}{I_2\theta_1} - 1\right\} + 1$$

From this the permeability of the specimen can be calculated, for different values of polarising field, It will be realised that the measurement used for equ. 27 could be dispensed with since it is merely a repeat of an earlier calibration measurement. It was regularly carried out, however, as it provided a routine calibration check.

By varying the polarising field in a cyclic manner and measuring the incremental permeability at various points on the cycle, a butterfly curve can be drawn as in fig. 15 (a). Values are tabulated in Table IV, Chapter IX.

When taking butterfly curves in this manner it was found that the curve was not symmetrical about the zero point of applied field: this was due to the earths vertical field (as the specimen was mounted vertically) which had a value of about 24 A/m (0.3 oersted). This seemed a rather high value and it was therefore checked, approximately, by mechanically turning the search coil through $180^{o}$. This was about 24A/m, within experimental error, which agreed with measurement using a vibration magnetometer. The high value is presumably due to the presence of a large amount of iron in the structure of/

of the laboratory in which these measurements were made.

When measurements of initial permeability were taken, a correcting field was therefore applied. It was difficult to be certain that complete cancellation had taken place, and several readings were therefore taken round about zero field strength and a mean value of permeability taken.

(c) Circular Permeability: Unsuccessful Methods.

At high frequencies the method used by the author to measure permeability employed a circular magnetic field, and it was therefore deemed desirable to make low frequency measurements with a similar configuration rather than the longitudinal field already mentioned. The first attempts were made using d.c. fields, as follows:

The apparatus consisted of a long brass tube (Fig.24) with the specimen mounted coaxially inside. This inner wire was insulated from the outer tube at one end and shorter to it at the other end. The variable resistor was set to give a suitable value of cument through the specimen. On switching this current off an induced e.m.f. was generated in the loop, formed by the inner and outer conductors, due to the collapse of the circular field in the wire and in the

air/

air space. This induced e.m.f. and the change in voltage drop in the resistance of the inner was fed, through a large capacity, to the ballistic galvanometer. Unfortunately, the deflection due to the resistance of the specimen completely swamped that due to the inductance and therefore a more complex method had t o be considered.

The most suitable method of overcoming the resistance effect of the specimen would be to employ a bridge circuit, and it was found that such a method had been employed by Kreielsheimer.[2] In this a Wheatstone Bridge is used in which the four arms are lecher lines. Two arms are identical and of non-magnetic material, the third arm is constructed of the magnetic specimen and the fourth arm of non-magnetic material whose resistance is equal to the specimen material. The bridge is supplied by D.C. and the detector (a ballistic galvanometer) reads zero. On switching off the supply, the inductances of the four arms do not balance and there will be a deflection on the galvanometer, due to the self inductance of the specimen wires. According to Kreiclsheimer the permeability can then be calculated from the following equation:

$$\mu = \frac{G_b R_x}{[2] I_3 l} \alpha \quad - \quad --- \quad \text{(c.g.s. units)}$$

where Gb = the galvanometer constant

Rx = the equivalent resistance of the bridge.

I4 = the current in arm 3.

2 = the factor of commutation.

$\alpha$ = the galvanometer deflection.

The present author attempted to repeat this experiment using coaxial lines in place of lecher lines. However, as Kreielsheimer noted, the results were very erratic, probably due to thermal e.m.f.s. in the circuit. Kreielsheimer attempted to remove these by immersing the apparatus in oil, without much success. Without going to that extent, the author also tried to obtain consistent results, but without any success.

If therefore seemed preferable to use an a.c. method where the inductance could be more easily separated from the resistance. The first method tried was similar to that in fig. 24 in which the batteries were replaced by an a.c. supply and the ballistic galvanometer by an oscilloscope. The separation of phase and amplitude changes

was/

was difficult, however, and another method was sought.

The author is indebted to Dr. J.S. Calderwood of the Electrical Engineering Department, Royal Technical College, for the suggestion that an a.c. potentometer could be used, and also for drawing his attention to the paper by Schelkumoff[29].

(d) Circular Permeability: A.C. Potentometer Method.

Instead of measuring the inductance of a coaxial line with the specimen as inner conductor the self inductance of the specimen may be measured when an alternating current is passed through it, and this is essentially, the method used here. The simplest method in theory which is, as it happens, a practical method, is to measure the voltage drop along the specimen with a known current passing through it.

This method was used by Hopps[30] in 1900, the voltage drop being measured by a hot-wire voltmeter. The magnitude of the impedence was measured at d.c. and at frequencies of 45, 66 and 100$^{c}$/s and was found to increase with frequency. Hopps called this impedance the apparent resistance and concluded,

"It/

"It is a matter for further experimenting to determine the nature of this additional resistance, in how far it is of a reactive nature and in how far it is of the nature of an ohmic resistance. A delicate wattmeter measurement would enable the resistance components to be separated and would be of still further interest in connection with the subject."

Fortunately an easier instrument than a wattmeter is now available; that is the a.c. potentometer, which measures both the real and imaginary components of the voltage.

The apparatus used by the author was D.C. Gall's Co-ordinate A.C. and Double D.C. Potentometer. The potential drop across the specimen (Fig. 25) was compared with the drop across the same length of eureka wire connected in series to a low voltage 50 c/s supply. Since the current through both wires was the same, the ratio of the two voltages is equal to the ratio of the impedances. In order to cut down stray flux linking the leads to the potentiometer, the specimen was enclosed in a $\frac{3}{8}$" dia. brass tube as used in previous experiments (fig. 24). This was connected to one end/

end of the specimen by a brass plug, the other end being insulated from the specimen. (The specimen was in effect, the inner conductor of a coaxial line). A twisted pair of leads from this end of the tube and the specimen completed the circuit to the terminals of the potentiometer. The eureka wire was connected, in a similar manner, to the second set of voltage comparison terminals. The brass tube, in addition to forming a circuit of low stray flux linkage, ensured that the length of the specimen was constant when the specimen was changed.

In order to find the impedance of the eureka wire so that it could be used for comparison, various resistive specimens were used. It was found in the specimens of high resistivity that the impedances were proportional to the d.c. resistances of the wires, i.e. their self inductances were negligible. Although exceptions were found when low resistance specimens (brass and copper) were used these were accounted for by the inaccuracy of measurement of low voltage drops. From this it will be appreciated that eureka was chosen as a reference specimen because its voltage drop is comparable with that of the magnetic specimens, thus increasing/

increasing the accuracy of the measurement.

The calculation of the impedance of the specimen can now be carried out, using the following symbols:

$Z_s$ = the surface impedance of the specimen

Reu = the resistance of the eureka wire, which was found, by measurement, to be 0.1799 ohms.

$V_s$ = the complex value of the specimen voltage drop.

Veu = " " " " eureka " "

$\hat{I}$ = the peak value of current through the specimen.

$\hat{H}$ = " " " " the polarising field

i.e. at the peak of the alternating field and at the outer radius, a, of the specimen.

Since the same current flows through the eureka and the specimen,

$$Z_s = R_{eu} \frac{V_s}{V_{eu}}$$

From this, the surface impedance of the specimen can be calculated and used, as will be described later, to find the complex permeability.

This permeability must be related to a value of field strength and it is convenient to take the maximum value i.e. the peak a.c. field at the surface of the specimen of/

of radius a:

$$\hat{H} = \frac{\hat{I}}{2\pi a} = \frac{\sqrt{2}\,|V_{eu}|}{R_{eu}} \times \frac{1}{2\pi a}$$

$$= 1{,}539\,|V_{eu}|\ A/m \quad \text{---} \quad (29)$$

when $R_{eu} = 0.1799$ ohm. and $a = 0.032$ in. (16 S.W.G.).

(e) Relation Between Permeability and Surface Impedance

The paper by Schelkunoff [29] on coaxial transmission lines and wave filters gives a very lucid description of the properties of circular waves along transmission lines and includes a discussion on the surface impedance of a wire. Although Schelkunoff's equations include a symbol for permeability, it is not a complex permeability and therefore the formulae only apply to materials of a non-magnetic character, since, at low and radio frequencies, all magnetic materials have a complex permeability, due to hysteresis loss. The following treatment is, in essence, that used by Schelkunoff, but the extension of the proof to complex permeability has greatly increased the difficulty of obtaining numerical solutions, and has made it necessary to make lengthy numerical calculations. The symbols used here are more in line with present day usage than Schelkunoff's and the M.K.S. rationalised/

rationalised system has been used: the fundamental formulae are the same as those in Skelkunoff's C.G.S. rationalised system, the difference lying in the values of $\mu_0$ and $K_0$.

The equations of the fields in a circularly propagated wave are:

$$E_r = \frac{\gamma}{g + j\omega\epsilon\epsilon_0} H_\phi$$

$$j\omega\bar{\mu}\mu_0 H_\phi = \frac{dE_z}{dr} + \gamma E_r$$

and $$\frac{d}{dr}(rH_\phi) = (g + j\omega\epsilon\epsilon_0) r E_z$$

where $\bar{\mu} = \mu_1 - j\mu_2$, the other symbols having their usual significance.

In a conductor, the specific inductive capacity, $\epsilon$, is zero and g, the conductance, can be replaced by $1/\rho$. There is no radial electric field, i.e. Er = 0.

Then $$j\omega\bar{\mu}\mu_0 H_\phi = \frac{dE_z}{dr} \quad - - - - \quad (30)$$

and $$\frac{d}{dr}(rH_\phi) = \frac{r}{\rho} E_z$$

ie. $$E_z = \frac{\rho}{r} \frac{d}{dr}(rH_\phi) \quad - - - \quad (31)$$

Substituting equ.(31) in (30),

$$\frac{d}{dr}\left[\frac{\rho}{r}\frac{d}{dr}(rH_\phi)\right] = j\omega\bar{\mu}\mu_0 H_\phi$$

By inspection of this equation, the solution may be written down, or else the left hand side may be expanded and the following equation reached

$$r^2 H''_\phi + r H'_\phi + (k^2 r^2 - 1) H_\phi = 0$$

where $k^2 = \frac{\omega \bar{\mu} \mu_o}{j \rho}$ and single and double priming denote the first and second derivatives respectively.

This is Bessel's Equation of order unity and the solution is therefore

$$H_\phi = A J_1(kr) + B K_1(kr)$$

$K_1$ tends to infinity as r tends to zero, but, in the practical case, $H_\phi$ tends to zero as r tends to zero: therefore $B = 0$.

Since the field at the outer radius a,

$$H_a = A J_1(ka) = \frac{I}{2\pi a}$$

then

$$A = \frac{I}{2\pi a J_1(ka)}$$

and equ. (31) becomes,

$$E_z = \frac{\rho}{r} \frac{d}{dr} \left[ r A J_1(kr) \right]$$

$$= \frac{\rho}{r} \cdot \frac{I}{2\pi a J_1(ka)} \cdot \frac{d}{dr} \left[ r J_1(kr) \right]$$

Now $$\frac{d}{dr}\left[r J_1(kr)\right] = k r J_0(kr)$$

hence $$E_z = \frac{k\rho I}{2\pi a} \cdot \frac{J_0(kr)}{J_1(ka)}$$

At radius a, $$E_z = \frac{k\rho I}{2\pi a} \cdot \frac{J_0(ka)}{J_1(ka)}$$

Then the surface impedance per unit length is

$$\frac{Z_s}{l} = \frac{E_z}{I} = \frac{k\rho}{2\pi a} \cdot \frac{J_0(ka)}{J_1(ka)}$$

i.e. $$Z_s = \frac{k\rho l}{2\pi a} \cdot \frac{J_0(ka)}{J_1(ka)}$$

Multiplying numerator and denominator by a gives,

$$Z_s = \frac{\rho l}{2\pi a^2} \cdot ka \cdot \frac{J_0(ka)}{J_1(ka)}$$

i.e. $$Z_s = \frac{R_s}{2}\left[ka\ \frac{J_0(ka)}{J_1(ka)}\right] \qquad \text{---------- (32)}$$

The values of $Z_s$ and $R_s$ (the d.c. resistance of the specimen) can be found by measurement and the value of the function inside the square bracket, which can be denoted by

$$S = |S| \angle \alpha = ka\ \frac{J_0(ka)}{J_1(ka)}$$

can be found. From this amplitude of ka, $|ka|$ , and its phase, $\phi$ can be calculated. This calculation presents rather a problem as the function S has to be calculated for several values/

values of ka and, by interpolation, the correct value found. As a large number of experimental results required to be calculated, it was found preferable to tabulate and plot the functions for the ranges required. The family of curves is shown in fig. 26 and the method of calculation and tabulated results are given in Appendix I

Thus for any measured value Za, the corresponding value of ka can be calculated.

Since $k^2 = \frac{\omega \bar{\mu} \mu_0}{j\rho}$ by definition,

then $(ka)^2 = \frac{a^2 \omega \mu_0 (\mu_1 - j\mu_2)}{j\rho}$

i.e. $\mu_1 - j\mu_2 = \frac{j\rho}{a^2 \omega \mu_0} (ka)^2$

The magnitude and the phase angle $(-\psi)$ of the complex permeability can then be found from

$$|\bar{\mu}| = \frac{\rho}{a^2 \omega \mu_0} |ka|^2 \quad \text{---} \quad (33)$$

and $-\psi = 2\phi + 90^\circ$

Measurements were made at various field strengths on different specimens and curves plotted of permeability against field strength. These are given in figure 47, the method of calculation being as follows.

(f)/

(f) Method of Calculation.

In order to simplify calculation, equ. 29 may be used with 32 and the definition of $|S| \angle\alpha$ to give

$$|S| \angle\alpha = \left[ka + \frac{J_o(ka)}{J_1(ka)}\right] = 2\frac{R_{eu}}{R_s} \cdot \frac{V_s}{V_{eu}}.$$

Since the length and diameter of the eureka and the specimen wire are, in most cases, the same, this may usually be simplified to

$$|S| \angle\alpha = 2\frac{\rho'_{eu}}{\rho'_s} \cdot \frac{V_s}{V_{eu}} \quad \text{---} \quad (34)$$

where $\rho'$ denotes the resistivity relative to copper. A sample calculation will now be made. Using a strand annealed mumetal specimen, the following results were taken on the a.c. potentiometer:-

$V_{eu} = 0.2302 + j.00232.$

and $V_s = 0.1811 - j.00272.$

In addition measurements using d.c. gave

$\rho'_{eu} = 27.64, \quad \rho'_s$ (mumetal) $= 36.35.$

For convenience of calculation the a.c. potentiometer voltages are converted to polar co-ordinates,

$V_{eu} = 0.2312 \angle 5^\circ 32'$

and $V_s = 0.1811 \angle -0^\circ 50'$

From/

From equ. 34, $S \angle\alpha = 2 \times \frac{36.35}{27.64} \times \frac{0.1811}{0.2312} \frac{\angle -0^\circ 50'}{\angle 5^\circ 32'}$

$= 2.061 \angle -6^\circ 22'$

From curves, $|ka| \angle\phi = 0.983 \angle -50^\circ$

From equ. 33,

$$|\mu| = \frac{\rho}{a^2 \omega \mu_0} |ka|^2 = 2,328 \times 0.983 = 2,245.$$

$$\psi = 2\phi + 90^\circ = -10^\circ$$

$$\therefore \bar{\mu} = 2,245 \angle -10^\circ = 2,200 - j390$$

From equ. 29,

$$\hat{H} = 1,539 \, |Veu| = \underline{278. \text{ A/m}}.$$

Thus strand annealed mumetal has a relative permeability of 2,200-j390 when subjected to a $50^c$/s field of peak strengths 278 A/m.

## CHAPTER VIII.

### MEASUREMENT OF D.C. RESISTIVITY.

In the calibration of the apparatus used for skin effect measurement (Chapter III) it is necessary to use the d.c. resistivity of various non-magnetic specimens. It is also desirable, for comparison, to know the d.c. resistivities of the magnetic specimens used. This chapter describes the method used to make these measurements.

A length of the specimen was drawn taut between two brass terminal blocks two feet apart, and held taut by screws. Two small voltage contacts were placed 50 cms apart on the wire and were connected to the voltage measurement terminals of a d.c. potentiometer. A second pair of test terminals on the potentiometer were connected to the voltage terminals of a 0.1 ohm shunt. This shunt was connected in series with the specimen to a low voltage, variable, d.c. supply and a set current passed through them. By measuring the voltages across them the resistances were compared and hence the specimen resistance calculated.

The results of the measurements on purely resistive materials are given in Fig.12 and on magnetic materials in Chapter IX.

CHAPTER IX

## RESULTS.

### (a) Microwave Resistivity and Permeability.

The results of the measurements described in Chapter V (d) are collected in the curves of figs. 27-32. The product $(\rho'\mu)$ of resistivity and permeability, relative to copper, to a base of polarising field strength (H) are given, for various materials, The field strength is the peak value of the polarising field, occuring at the surface of the specimen. In general, specimens were tested in three different states:

(1) Strand Annealed (black curve): This means that the specimen was annealed in a coil before leaving the works. Any subsequent working due to straightening and cutting the specimen would alter this state.

(ii) Annealed (red curve): These specimens were annealed in suitable lengths (short lengths of about 10 in. for microwave measurements and lengths of about a yard for low frequency and d.c. measurements). The specimens for both low and high frequency measurements/

measurements were annealed together to obtain similar conditions. They were hung in a vertical furnace with nitrogen passing over them to reduce oxidation. The specimens were annealed as follows:

RADIOMETAL and MUMETAL; over 800°C for more than one hour after which time they were removed slowly, taking about five minutes,

RHOMETAL; 800°C for half an hour, removed quickly.

OTHER SPECIMENS; 600°C for twenty minutes, removed in about one minute.

(iii) Annealed, Cleaned and Polished (green curve): A specimen treated as in (ii) was cleaned with emery cloth and polished with jewellers rouge. It must be remembered that this will cause not only a change in resistivity due to the change in the surface but also a change in permeability due to the working of the specimen.

From these curves it is possible to make an estimate of resistivity (i.e. the value of $\rho'\mu$ as the permeability tends to unity). The approximate error in this estimate, due to the difficulty of extrapolating accurately, is given in table III, column 6. This will be discussed further in the following chapter. The estimated value/

TABLE III Results of Microwave and D.C. Measurements.

| SPECIMEN | A<br>Relative Resistivity (d.c.) | B<br>$\rho'\mu$ at H = 0 | C<br>$\rho'\mu$ as $\mu \to 1$ | $\mu = \frac{B}{C}$ | Appx. Error due to difficulty of saturating | D.C. Initial Permeability |
|---|---|---|---|---|---|---|
| RADIOMETAL | 45.3 | 2090 | 60 | 35 | + 43%<br>- 0 | 594 |
| (Ann & Cleaned) | " | 1170 | Indeterminate | - | - | 1400 |
| (Annealed) | " | 1130 | 160 | 7.06 | ± 25% | " |
| RHOMETAL | 43.0 | 1495 | 110 | 13.6 | ± 15% | 241 |
| (Ann & Cleaned) | " | 640 | 120 | 5.33 | ± 10% | 1230 |
| (Annealed) | " | 564 | 70 | 8.03 | ± 20% | " |
| MUMETAL | 36.3 | 638 | 60 | 10.6 | ± 5% | 1720 |
| (Ann & Cleaned) | 37.3 | 182 | 36 | 5.06 | ± 6" | 5840 |
| (Annealed) | " | 317 | Indeterminate | - | - | " |
| STEEL | 10.7 | 440 | 20 | 22 | ± 50% | 70 |
| (Ann & Cleaned) | 10.5 | 587 | 25 | 23.5 | ± 8% | 114 |
| (Annealed) | " | 958 | 30 | 31.9 | ± 30" | " |
| IRON | 6.63 | 269 | 40 | 6.72 | ± 15" | 190 |
| (Ann & Cleaned) | 6.73 | 244 | 25 | 9.76 | ± 30% | 200 |
| (Annealed) | " | 760 | order of 100 | order of 7.6 | high | " |
| NICKEL | 7.74 | 81.9 | 9 | 9.01 | ± 10% | 24 |

value of permeability, together with information regarding values of initial permeability and resistivity, is listed in table III. The measurements were carried out at a wavelength of 10.43 cms ($2870^{MC}/S$).

(b) Static Longitudinal Permeability.

The method of measuring the initial longitudinal permeability has been described at the end of section VII (b). Results are given in table III.

(c) D.C. Resistivity.

The d.c. resistivity was measured as described in Chapter VIII and the resistivity of magnetic specimens relative to copper are given in table III.

(d) Butterfly Curves at D.C.

The method of taking D.C. butterfly curves has been described at the end of section VII (a). In brief, it may be said that a longitudinal d.c. polarising field is superimposed on a low amplitude d.c. field. This low amplitude field is reversed and a ballistic measurement of permeability is made. By taking a cycle of readings with a field varied between +1960 A/m and -1960A/m, butterfly curves can/

can be drawn similar to that sketched in fig. 16(a). The characteristic points of these curves are tabulated in Table IV, the symbols referring to fig 16 (a).

(e) Butterfly Curves at Microwaves: Circular and Longitudinal Polarising Fields.

A point by point butterfly curve for mumetal was taken, using a microwave field for measurement, with a variable d.c. field as polarising field. The range of polarising field was that used in the previous section ($\pm$ 1960 $^{A}/m$) and the results are tabulated in table IV. It should be noted that, here, the results are of the product of resistivity and permeability.

Using the photographic technique described in Chapter VI, butterfly curves, figs. 33-43, were taken. For a similar specimen to the above, fig. 37 (a) shows that an initial $\rho'u$, of 454 is altered by 268 on applying the same field as above. This is in close agreement with the point by point method. The calculation is described in section VI (d). For each specimen three photographs are given:

(a) With an alternating circular field of 1,960 $^{A}/m$ peak/

TABLE V BUTTERFLY CURVES: PHOTOGRAPHIC METHOD.

| SPECIMEN | Initial $\rho'\mu$ | Circular Field $\delta(\rho\mu)$ | % | Longitudinal Field $\delta(\rho\mu)$ | % | Longitudinal + Circular Field $\delta(\rho\mu)$ | % |
|---|---|---|---|---|---|---|---|
| RADIOMETAL | 2080 | 460 | 22 | 8320 | 400 | 8600 | 413 |
| Annealed | 3390 | negligible | | 2090 | 62 | 2180 | 64 |
| RHOMETAL | 1620 | 300 | 19 | 4880 | 302 | 4190 | 258 |
| Annealed | 4350 | negligible | | 5100 | 118 | 6200 | 143 |
| MUMETAL | 454 | 268 | 59 | 8300 | 1830 | 8600 | 1900 |
| Annealed | 365 | 192 | 53 | 101 | 28 | 305 | 84 |
| IRON | 341 | 25 | 11 | 277 | 120 | 305 | 132 |
| Annealed | 606 | 67 | 11 | 474 | 78 | 541 | 89 |
| STEEL | 293 | 37 | 13 | 347 | 118 | 411 | 140 |
| Annealed | 872 | 202 | 23 | 1248 | 143 | 1488 | 170 |
| NICKEL | 79 | 29 | 37 | 69 | 87 | $>71$ | $>90$ |

peak field in each direction at the surface of the specimen.

(b) With an alternating longitudinal field of 1960 $^{A}/_{m}$ peak in each direction.

(c) With an a.c. longitudinal field as in (b) and a superimposed d.c. circular field of 1960 A/m at the surface of the specimen.

It will be realised that a fourth photograph could be taken using an a.c. circular field with a superimposed d.c. longitudinal one. Examples of this are given in figs. 21 (b) and (c) which show that the tendency of the applied d.c. field is to reduce the curve to zero. In fact, in all the specimens tested, it was found that if the same field values as were usedin (iii) above were employed, the curve degenerated to a straight line. There is, thus, no point in adding a fourth photograph to the series.

The figures for the unpolarised value of, and the change in, the product of resistivity and permeability ($\rho'u$) are given below each photograph and are tabulated in Table V.

(f) Circular Permeability at 50 $^{C}/_{S}$.

This was measured by the method described in section/

## TABLE VI Representative Values of Circular Permeability.

Note: Permeability is defined by $|\mu| \angle -\varphi = \mu_1 - j\mu_2$, hence when $-\varphi$ and $\mu_2$ are positive the vector lies in the fourth quadrant, when they are negative the vector is in the first quadrant.

| | D.C. Initial Permeability | Lowest Value of H | | | | | Highest Value of H | | | | | Peak Permeability | | | | |
|---|---|---|---|---|---|---|---|---|---|---|---|---|---|---|---|---|
| | | H A/m | $\mu_1$ | $\mu_2$ | $\lvert\mu\rvert$ | $-\varphi^\circ$ | H A/m | $\mu_1$ | $\mu_2$ | $\lvert\mu\rvert$ | $-\varphi^\circ$ | H A/m | $\mu_1$ | $\mu_2$ | $\lvert\mu\rvert$ | $-\varphi^\circ$ |
| RADIOMETAL | 594 | 19.2 | 341 | -160 | 377 | -25.0 | 286 | 720 | 248 | 762 | 19.0 | - | - | - | - | - |
| Annealed | 1,400 | 19.2 | 1,451 | 126 | 1,456 | 5.0 | 286 | 2,856 | 1,097 | 3,059 | 21.0 | 167 | 3,373 | 1,546 | 3,710 | 24.6 |
| RHOMETAL | 241 | 75 | 292 | -169 | 338 | -30.0 | 278 | 580 | 102 | 588 | 10.0 | - | - | - | - | - |
| Annealed | 1,230 | 21.5 | 1,118 | 104 | 1,122 | 5.3 | 279 | 2,502 | 1,129 | 2,730 | 23.6 | 200 | 2,652 | 1,247 | 2,930 | 25.2 |
| MUMETAL | 1,720 | 15.3 | 2,129 | 224 | 2,141 | 6.0 | 279 | 2,211 | 390 | 2,245 | 10.0 | 85 | 3,700 | 1,600 | 4,000 | 23.4 |
| Annealed | 5,840 | 17 | 9,532 | 3,987 | 10,330 | 22.7 | 281 | 2,882 | 384 | 2,915 | 7.6 | 24.6 | 10,280 | 4,905 | 11,400 | 25.5 |
| IRON | 190 | 55 | 250 | 32 | 252 | 7.2 | 284 | 629 | 286 | 692 | 24.4 | - | - | - | - | - |
| | | MEAN VALUE | | | | | | | | | | | | | | |
| STEEL | 70 | - | 39.1 | 87.8 | 96.1 | 66.0 | | | | | | | | | | |
| NICKEL | 24 | - | 27.2 | 15.5 | 40.3 | 22.6 | | | | | | | | | | |

section VII (d). Results for strand annealed and annealed specimen are given, for applied fields up to 300 $^{A}/m$ in figs 44-47. Owing to the low voltage drop along the specimen at low values of field strength, it was not possible to measure initial values of permeability. Representative values are therefore quoted in table VI.

It will be seen that there are no curves for nickel or steel. In both cases the results were fairly steady and the mean value has been given.

(g) Calibration of Microwave Apparatus.

Table VII gives sample measurements, taken as a series, which have been averaged with other sets taken at different times, to plot fig. 12.

TABLE VII - Calibration Using Resistive Materials.

| Specimen | Galvanometer Reading | Ratio to Copper (12.8) | Q ratio | Square root of d.c. resistance relative to copper |
|---|---|---|---|---|
| Copper (reference) | 12.8 | 1.000 | 1.000 | 1.00 |
| Brass | 11.8 | 1.085 | 1.042 | 1.97 |
| Tantalum | 10.4 | 1.280 | 1.130 | 2.94 |
| Eureka | 8.4 | 1.525 | 1.235 | 5.36 |
| Brightray | 6.6 | 1.940 | 1.390 | 8.09 |

CHAPTER X

## DISCUSSION OF RESULTS

Dealing first of all with the results of the microwave permeability measurements; in general the results for the annealed and strand annealed states appear satisfactory, but the annealed and cleaned state gives a curve which lies sometimes between the two results e.g. rhometal , and sometimes not, e.g. iron. Naturally, when the specimen is being cleaned, the working causes it to become "hard", magnetically, and since the amount of this varies from specimen to specimen, the relative position of the annealed and cleaned specimen will be indeterminate.

The accuracy of these measurements is, probably, $\pm$ 10% to $\pm$ 20% for the product of resistivity and permeability. In addition, when the permeability is calculated, there is an indeterminacy in the value of resistivity due to the difficulty of saturating the specimen. The error introduced from this source has been tabulated in Table III, Chapter IX. In drawing the curves, however, the first mentioned errors are smoothed out and can be reduced. It would therefore seem that an accuracy of $\pm$ 30% could be claimed for most of the/

the results in Table III.

In fig.29 the shape of the curve for annealed mumetal appears unsatisfactory. It would seem, from its linear nature, that an impure layer, composed of a mixture of magnetic and non-magnetic particles, had formed. In this particular case the cleaned and annealed specimen was therefore taken as representative of the annealed state.

The effect of annealing is that, in the lower permeability materials, iron and steel, annealing raises the permeability. In the higher permeability materials it is seen from the curves and Table III that the position is reversed. This was unexpected, but checks on the high permeability materials showed that there was no reason to doubt the results. Further comments on this will be made in Chapter XI.

The accuracy of the d.c. longitudinal permeability measurements is about $\pm$ 1% while the d.c. resistivity measurements were taken to greater accuracy than that, but have been quoted to the third significant figure only.

The measurements of permeability at $50^{c}$/s using a circular field (figs. 44-47) and those with a d.c. longitudinal/

longitudinal field shows that the change of permeability with annealing is normal in both cases; i.e. the permeability is higher in the annealed state. This means that for the higher permeability materials the position changes at some point below 3,000 $M^c/s$.

The voltage measurements for the $50^c/s$ circular permeability experiments were taken to the fourth significant figure, but, due to supply voltage and frequency,variations, it is unlikely that an accuracy of better than 1% can be claimed for the vector voltage ratio. As the results were taken in the evening while the supply was fairly stable, the accuracy may, in fact be better. Due to the intricate relationship between this voltage ratio and the permeability, it is not possible to judge the effect on the permeability. As an example, a change in the complex voltage ratio of $0.12^o$ (no change in the magnitude of the ratio) causes a change of 3% in the permeability and $0.2^o$ in a phase of $5^o$. A change of 0.3% in the magnitude of the ratio causes a 1% change in the permeability with $1^o$ in a phase of $25^o$. These examples were taken from the calculations leading to the plotting of fig.45 for rhometal.

The/

The results of strand annealed radiometal in a circular field show a change of quadrant at low values of field strength. The fact that a smooth curve can be drawn through the points and the fact, not visible on the curves, that the first seven points at low field strength were so close that a mean value was taken, point to these results being correct. However this only demonstrates that the result is repeatable and does not necessarily guarantee its absolute accuracy. In fact, if the magnitude of the voltage ratio is 1% low the curves would be raised so that there would not in fact be the quadrant change mentioned. Unfortunately, due to the time taken to work out the results it was not possible for the author to repeat these measurements under different conditions. Since it is the first time that measurements of this type have been made, at least to the author's knowledge, it is hoped that these comments will be of assistance to anyone extending the measurements, or repeating them with more accurate instruments.

Another point of interest in these measurements is that in general the value of circular permeability, is higher than the initial permeability measured with a longitudinal field (Table VI). The field used in the circular permeability is higher than that used for the initial permeability/

permeability measurements, which in itself would account for the difference. Radiometal is again the exception. As the steel and nickel results are fairly constant and have been averaged, it may be assumed that they are initial values for circular fields, and that they can be directly compared with the longitudinal values. This comparison shows that the amplitude of the circular permeability is still higher than the longitudinal value in both cases.

The butterfly curves taken at microwaves have an accuracy of about $\pm$ 10% to 20% The percentage changes in permeability caused by the application of standard field strengths occur in the following orders:-

(i) Circular Field

Strand annealed Specimen; iron, steel, rhometal, radiometal; mumetal.

Annealed Specimen; radiometal, rhometal, iron, steel, nickel, mumetal.

(ii) Longitudinal Field.

Strand annealed Specimen; steel, iron, rhometal, radiometal, mumetal.

Annealed Specimen; mumetal, radiometal, iron, nickel, rhometal/

rhometal, steel.

The Strand Annealed Specimens show very similar results for circular or longitudinal fields. In fact the slight differences in order are accountable by inaccuracy in the results. The annealed specimens show no similarity.

When the results of the butterfly curves using combined fields (c) are compared with those for longitudinal fields (b) the orders are the same for both annealed and strand annealed specimens. This is not surprising since the effect of the d.c. polarising field is small compared with that of the a.c. field.

## CHAPTER XI

## CONCLUSIONS

The microwave measurements have shown the practicability of the method used. It is difficult to saturate the material, or to be certain that it is saturated. Measurements at lower radio frequencies might throw light on this problem, since the R.F. and d.c. resistivities could be considered the same.

When, in section IV(d), the method of calculating the permeability changes from the photographs of butterfly curves was described, two important points were made. Firstly, in the case of a circular polarising field, the initial value of the product of resistivity and permeability is, approximately, the peak value of the butterfly curve. This is the usual variation of permeability with respect to polarising field; as the field increases, the permeability decreases and, presumably, the resistance stays constant. In the second case, with a longitudinal polarising field, the maximum value of the product of resistivity and permeability occurs at the maximum value of field strength. It would appear that this increase is caused by an increase

of/

of resistivity due to the polarising field field which is perpendicular to the microwave magnetic field used for measurement.

This effect of a magnetic field on the resistance of a material has been discussed, for low frequency measurements, by Bates[31] who states that the effect of a polarising field perpindicular to the measuring field is to decrease the resistance. This is the opposite to what the author has found in the microwave measurements, but then, other properties are different at these frequencies. In addition, Bates mentions that parallel fields also affect the resistivity. This could cause unexpected errors in the measurements of permeability at microwaves, which have been described: but it should be noted that it in no way affects the results of the product of resistivity and permeability, especially the photographs and calculated results of Chapter VI. This would point to the desirability of further checks on the method at lower frequencies and these will be discussed later in this chapter.

The microwave measurements of Hodsman et al[21] cover a wide frequency range, but their measurements assume that the/

the resistivity to d.c. is the same as that to microwave currents. Their results for iron and steel, which follow, are higher than the author's, at the same frequency, the author's results being given in brackets:- steel, 59(22); annealed steel, 43(31.9); iron 62(6.7); annealed iron, 60(7.6). If the resistivity of the material is assumed to be that at d.c., the author's results for steel and iron become 40.5 and 41.2, respectively; it is pointless to give the figures for the annealed specimens as the surface of the wire was radically altered. The results for nickel are not directly comparable as the same frequency has not been covered. However, at a slightly higher frequency Hodsman et al have a result of 8.3 which, with the tendency of the curve taken into account, is very close to the author's result of 9.

The effect of annealing the specimens has already been mentioned in Chapter X. In the microwave measurements, the high permeability materials were found to have lower permeabilities when annealed. The results of iron and steel appear different but, if the accuracy of the measurements is taken into account, it will be seen that it is

just/

just possible that these low permeability materials exhibit the same feature. This statement seemed to disagree with results found by others, for example Hodsman et al[21] who say that, like Arkadiew, they found that annealing increased the permeability, even at high frequencies. This statement is not borne out by their results which have been plotted in fig.48 where it is seen that for steel and iron, the only materials given in both states, the annealed permeability is lower up to about 5,000 $M^c/s$, above which the situation returns to that at low frequencies.

The experiments and results described in this thesis contain several points which have not previously received attention; they also indicate subjects where further work, is desirable. The circular permeability has not previously been measured at low frequency for comparison with the microwave permeability; in fact, it does not appear to have been realised that the field configurations are different in the usual l.f. and microwave measurements. It should be pointed out that Kreielsheimer[2] had realised the position when making h.f. measurements. Kreielsheimer's method was not very satisfactory and the method which has been described here/

here is more dependable and should be suitable for measurements over the audio frequency range.

Further work could yet be done using this method, especially with respect to polarising fields. It should be fairly easy to apply a longitudinal magnetising field to the specimen, while measurements are being made with the potentiometer. It would be somewhat more difficult to apply a circular polarising field as blocking condensers would be required. At $50^{c}/s$ these would require to be very large and it is unlikely that electrolytic condensers could be used, due to the e.m.f. set up in the electrolyte. The use of a higher measurement frequency might make this problem easier. Assuming that some way of overcoming this difficulty could be found, a study could be made on the effect of saturation on the resistivity of the material, providing a check on the basic assumption used both in this thesis and the experiments of Johnson and Rado[20]. When the author started the research work described here, it seemed that the field of low frequency measurements offered no scope for original work, but it is now realised that in addition to the experiments carried out, there is still scope for further research along the lines mentioned above.